Pergamon

Geochimica et Cosmochimica Acta, Vol. 67, No. 6, pp. 1229–1245, 2003

0016-7037/03 $30.00 + .00

doi:10.1016/S0016-7037(02)01286-3

# The distribution of mantle and atmospheric argon in oceanic basalt glasses

MARIO TRIELOFF,[1,*] MARTINA FALTER,[2] and ELMAR K. JESSBERGER[3]

[1]Mineralogisches Institut der Universität Heidelberg, Im Neuenheimer Feld 236, D-69120 Heidelberg, Germany
[2]Max-Planck-Institut für Kernphysik, Saupfercheckweg 1, D-69117 Heidelberg, Germany
[3]Institut für Planetologie, Wilhelm-Klemm-Str. 10, D-48149 Münster, Germany

(*Received June* 11, 2002; *accepted in revised form October* 11, 2002)

**Abstract**—Argon analyses by both high-resolution stepheating and stepcrushing of MORB and Loihi basalt glasses were performed to separate pristine mantle-derived Ar and contaminating atmospheric Ar. In high-vesicularity glasses ($>$ 0.8% vesicles), most of the mantle argon resides in vesicles, from which it is released by crushing or stepheating between 600 and 900 °C. By contrast, in low vesicularity glasses ($<$ permil vesicularity), most mantle argon is dissolved in the glass matrix, as inferred from the correlation with neutron-induced, glass-dissolved argon isotopes ($^{39}$Ar, $^{37}$Ar, $^{38}$Ar from K, Ca, Cl). The distribution of mantle Ar between vesicles and glass matrix is well explained by melt-gas equilibrium partitioning at eruption according to Henry's law, which is compatible with previously determined Henry constants of $\sim$(5–10) $\times$ $10^{-5}$ccSTP $^{40}Ar_{mantle}$/g bar. Atmospheric Ar is heterogeneously distributed in all samples. Only a very minor part is dissolved in the glass matrix; a significant part correlates with vesicularity and is released by crushing, most probably from a rather small fraction of vesicles or microcracks that equilibrated with unfractionated air. Other carriers of atmospheric argon are pyroxene microlites and minor phases decomposing at intermediate temperatures that were probably contaminated upon eruption by fractionated atmospheric rare gases. Our high-resolution stepheating and stepcrushing analyses of low vesicularity samples with extraordinary high solar-like $^{20}$Ne/$^{22}$Ne indicate successful discrimination of unfractionated air as a contamination source and suggest an upper mantle $^{40}$Ar/$^{36}$Ar of 32,000 $\pm$ 4000 and a Hawaiian mantle plume source $^{40}$Ar/$^{36}$Ar ratio close to 8000. 

## 1. INTRODUCTION

Noble gas geochemistry is a tool to obtain information about the early history and composition of the Earth and also about present-day processes that otherwise are inaccessible (Ozima and Podosek, 2002). For example, the occurrence of solar-type He and Ne in the Earth's mantle (Clarke et al., 1975; Craig and Lupton, 1976; Sarda et al., 1988; Honda et al., 1991; Hiyagon et al., 1992) demonstrates that the Earth acquired solar gases during accretion, either by direct capture from the solar nebula (Hayashi et al., 1979; Pepin, 1991; Porcelli et al., 2001) or by solar wind implantation (Wetherill, 1981; Trieloff et al., 2000, 2002). Excess of radiogenic nuclides in the mantle sources ($^{40}$Ar from $^{40}$K, $^{4}$He and $^{21}$Ne from U and Th, $^{129}$Xe from short-lived $^{129}$I, and fission xenon from $^{238}$U and short-lived $^{244}$Pu) indicate early massive mantle degassing and bear important constraints on the evolution of the early terrestrial atmosphere (Allègre et al., 1986; Turner, 1989; Ozima, 1994). Finally, noble gas isotopic differences between the MORB mantle and high $^{3}$He/$^{4}$He mantle sources such as Hawaii are closely related to the structure and evolution of the Earth's mantle. This contributes to the discussion of whether mantle plumes are associated with deep reservoirs that are less degassed and less depleted than the upper mantle and whether their existence requires layered (or admits whole) mantle convection models (Porcelli and Wasserburg, 1995; Hofmann, 1997; Kellogg et al., 1999).

Progress toward answering these important questions depends exclusively on a better evaluation of actual noble gas isotopic compositions in the Earth's mantle, i.e., the composition of primordial isotopes as well as the magnitude of excess radiogenic rare gas nuclides from short- and long-lived precursors. Knowledge about noble gases in the Earth's mantle needs analyses of mantle-derived rocks, in particular, the rapidly chilled glassy rims of submarine basalts where mantle noble gases are preserved (Dalrymple and Moore, 1968; Fisher, 1971; Ozima, 1975; Kumagai and Kaneoka, 1998). However, more than two decades research has demonstrated the ubiquitous presence of atmosphere-derived contaminating noble gases (Ne, Ar, Kr, Xe) that obliterate or at least dilute the mantle signal, but the nature of the contamination process as well as possible carrier phases are not well constrained. Hence, advancing our understanding of contamination processes and carriers is of major importance in view of improving techniques to better isolate the mantle endmember component in future analyses.

The effect of contamination can be demonstrated in a neon three-isotope plot (Fig. 1). MORB and Loihi (Hawaii) basalt glass data form mixing lines that reflect mixing between the upper mantle or plume source neon with high $^{20}$Ne/$^{22}$Ne ratios of solar composition of either 12.5 (solar wind-implanted Ne-B: Black, 1972; Trieloff et al., 2000) or 13.8 (unfractionated solar gas: Honda et al., 1991; Benkert et al., 1993) and atmospheric composition ($^{20}$Ne/$^{22}$Ne = 9.8). In fact, many basalt glasses are very close to the atmospheric value (as plotted samples S2341–2 and 2ΠD44), while the minority of samples, particularly Loihi basalt glasses (e.g., S2335-6 and 10, 2ΠD43 and 40) have close to solar $^{20}$Ne/$^{22}$Ne ratios. High $^{20}$Ne/$^{22}$Ne values are roughly correlated with mantle source radiogenic excess (high $^{40}$Ar/$^{36}$Ar or high $^{129}$Xe/$^{130}$Xe); how-

* Author to whom correspondence should be addressed (trieloff@min.uni-heidelberg.de).

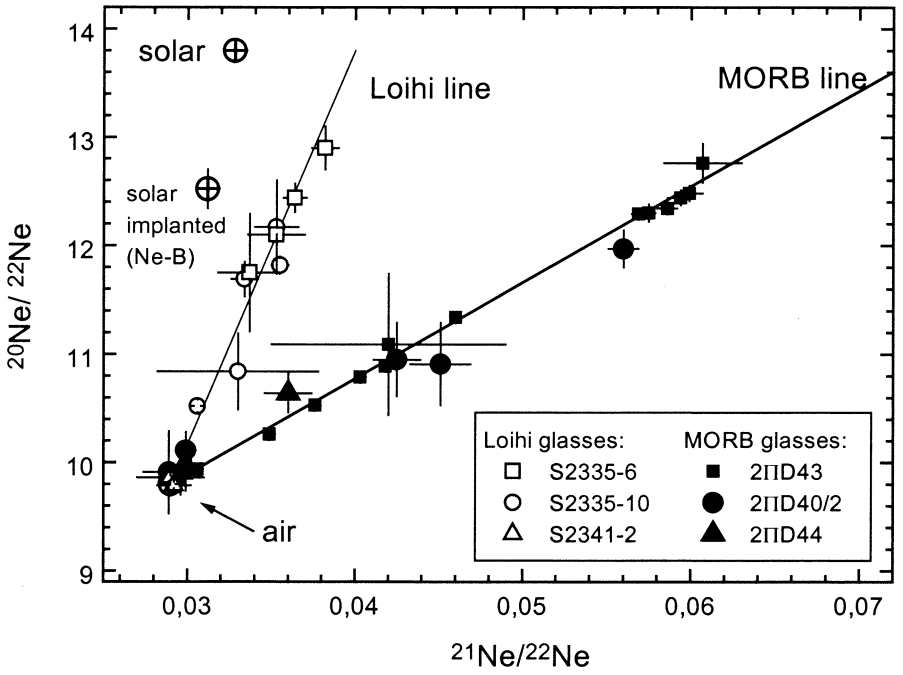


Fig. 1. Ne isotopic composition from basalt glasses used in this study. MORB glass data: Sarda et al. (1988), Moreira et al. (1998). Loihi glass data: Valbracht et al. (1997). Data cover nearly the complete $^{20}Ne/^{22}Ne$ range between mantle endmember (solar) composition and (contaminating) air.

ever, in many cases correlations are not very well defined, thereby limiting the use of neon isotope ratios as proxies for Ar or Xe contamination (Moreira et al., 1998; Trieloff et al., 2000, 2002).

It is clear that the atmospheric noble gas component is heterogeneously distributed within single samples, as inferred by the variation of single sample data along the mixing lines in Figure 1. Moreover, there is general agreement that atmospheric noble gases are not simply adsorbed air that should likely be removed by laboratory procedures (mainly in vacuo sample preheating for several days at 200 °C). There had been different suggestions concerning the location of the atmospheric contaminant. For example, it was argued that it is dissolved in the glass matrix, while $CO_2$ vesicles contain the pristine mantle rare gases (Marty et al., 1983; Jambon et al., 1985; Marty and Ozima, 1986). These studies suggested contamination upon eruption in interaction with seawater, a view also supported by Patterson et al. (1990). However, crushing experiments have shown that a significant fraction of atmospheric noble gases resides in vesicles (Fisher, 1994; Moreira et al., 1998; Harrison et al., 1999; Trieloff et al., 2000, 2002; Althaus et al., 2003). Ballentine and Barfod (2000) inferred a correlation of vesicularity and the presence of atmospheric noble gases with elemental ratios indistinguishable from unfractionated air in both submarine and subglacially erupted basalt glasses. They suggested late air-sample interaction as a responsible process, possibly because of incorporation of atmospheric noble gases into opened and resealed microfractures when handling the samples. Nevertheless, atmosphere-derived components fractionated similarly to deep seawater or sediments have also been observed (Harrison et al., 1999, 2002; Trieloff et al., 2000, 2002; Althaus et al., 2003) and should be considered as well. Finally, a better understanding of contamination processes should also help in evaluating models suggesting that correlations of atmosphere-like noble gases and enriched Pb isotopes indicate subduction of atmosphere-type gases rather than local recent contamination (Sarda et al., 1999; Burnard, 1999).

As in some previous studies, we focus on argon that can be analysed with much higher resolution. This is because of high abundances and isotopic variability, i.e., excess of radiogenic $^{40}Ar$ relative to air ($^{40}Ar/^{36}Ar = 295.5$) that is orders of magnitude higher in the Earth's mantle. However, the highest $^{40}Ar/^{36}Ar$ ratios obtained so far by stepheating and crushing basalt glasses are found only in a few samples, reflecting the severe contamination discussed above. For our study, we used MORB glasses (popping rock 2ΠD43, 2ΠD40) and Loihi glasses (S2335-6, S2335-10) that yielded the highest $^{20}Ne/^{22}Ne$ and $^{40}Ar/^{36}Ar$ ratios obtained so far (Staudacher et al., 1989; Burnard et al., 1997; Valbracht et al., 1997; Moreira et al., 1998). For comparison, three other samples (MORB glasses CYP7806-11, 2ΠD44 and Loihi glass S2341-2) were selected with intermediate-to-severe atmospheric contamination.

$^{40}Ar/^{36}Ar$ mantle source estimates derived from these samples are still not straightforward. Valbracht et al. (1997) measured the Loihi glasses mentioned above (Fig. 1) that are exceptionally pristine samples collected by a submersible at the southern rift zone of the Loihi seamount in 3- to 5-km depth. They suggested a $^{40}Ar/^{36}Ar$ source estimate between 2500 and 6000 for the Hawaiian mantle plume, which may be compared with the recently inferred value of 8000 from Loihi dunites (Trieloff et al., 2000). Analyzing the gas-rich popping rock 2ΠD43, Burnard et al. (1997) suggested $^{40}Ar/^{36}Ar > 40{,}000$ for the upper mantle, while Moreira et al. (1998) argued for a

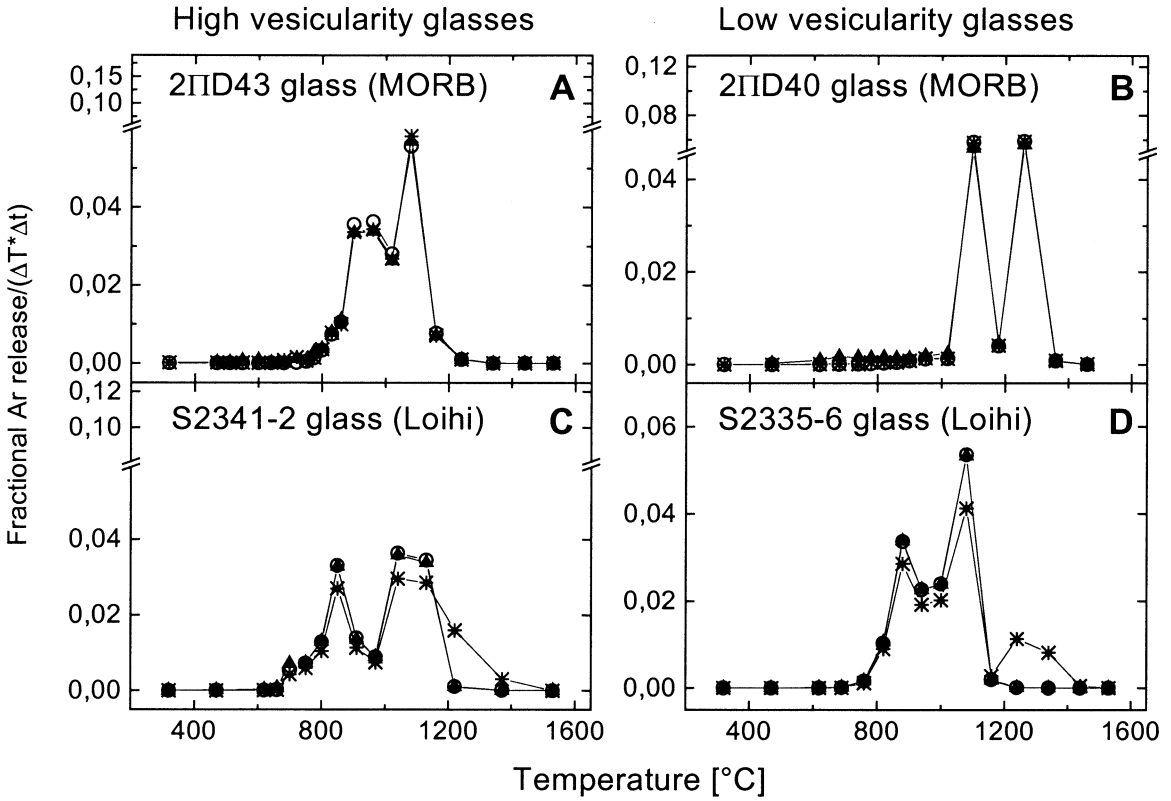


Fig. 2. Release of neutron-induced Ar isotopes (% $K^{-1}min^{-1}$) from low and high vesicularity MORB and Loihi glasses (on same scale as Fig. 4 for better comparison). $^{39}Ar$ from K: open circles; $^{37}Ar$ from Ca: stars; $^{38}Ar$ from Cl: solid up triangles. Note the nearly indistinguishable release of isotopes from different precursor elements, indicating that all three neutron-induced isotopes are distributed homogeneously in the glass. Exception is $^{37}Ar$ release at $>$ 1200 °C from Loihi glasses due to release from Ca-rich pyroxene microcrysts. The two-peaked release pattern of the glass matrix is observed for all samples.

value between 25,000 and 44,000. It may be questioned if popping rock 2ΠD43 can be used to infer upper mantle noble gas composition, as it was sampled from a geochemical and bathymetric anomaly and is presumably E-MORB. However, its general noble gas isotopic composition (Staudacher et al., 1989; Kunz et al., 1998; Moreira et al., 1998) is typical for worldwide MORB samples: It matches the mean MORB $^{3}He/^{4}He$ value of $\sim$8 $R_A$. In the neon three-isotope plot (Fig. 1); it coincides perfectly with the MORB line that was originally defined by data of Sarda et al. (1988) for worldwide MORB samples, and it also agrees with the $^{129}Xe/^{130}Xe$ vs. $^{136}Xe/^{130}Xe$ correlation line of worldwide MORB samples. Contrary to popping rock 2ΠD43, MORB glass 2ΠD40 was sampled from a topographic deep (4620-m depth) more than 100 km to the north.

The goal of our study is not only to improve knowledge on contamination sites and processes, but also to improve isolation of the mantle component by using rather uncontaminated samples. In addition, we anticipated increasing this effect by working with a much higher resolution than hitherto used (cf. Jessberger et al., 1974), i.e., extracting argon with up to 22 instead of the typical three steps. Finally, we follow up with a novel approach initially used for diamonds (Turner et al., 1990) and peridotitic rocks (Trieloff et al., 1997) to monitor Ar release from K-, Ca-, and Cl- bearing phases in mantle-derived rocks: Before argon extraction by stepwise heating and mass spectrometric analyses, basalt glass samples were neutron-irradiated (as for $^{40}Ar$-$^{39}Ar$ dating), thereby inducing argon isotopes $^{39}Ar$, $^{37}Ar$, and $^{38}Ar$ from K, Ca, and Cl, respectively. Their release pattern during incremental heating characterise Ar components homogeneously distributed within the glass (or possibly other minor K-, Ca-, or Cl-rich phases), allowing tracing of natural (i.e., mantle or atmospheric) argon components dissolved in the glass.

## 2. SAMPLES AND EXPERIMENTAL PROCEDURES

After gentle crushing, fresh and clean glass fragments of $\sim$3 to 7 mm in size were selected for argon isotopic analysis. Some of the glass fragments showed surficial covers of palagonite or manganese oxide crusts. All fragments were cleaned ultrasonically with diluted nitric acid, quartz distilled water, and ethanol. Subsequently, they were checked under the binocular for remnants of alteration products. Persistent alteration remnants were removed mechanically with dental drill equipment and cleaned again as described above. Thin sections of single fragments were prepared to determine vesicularity by petrographic point counting. Broken vesicles at glass boundaries in thin sections were not counted, as argon from such opened vesicles is lost during sample preparation of subsamples for

Table 1. Summary of Ar data obtained by stepwise heating and crushing of MORB and Loihi glasses.

| Glasses | Sample weight [mg] | Eruption depth[a] [m] | Number of extractions | $^{40}Ar_{tot}$ [$10^{-8}$ccSTP/g] | $^{40}Ar_{mantle}$ [%][b] | $^{40}Ar/^{36}Ar_{tot}$ | $^{40}Ar/^{36}Ar_{max}$ | $(^{40}Ar/^{36}Ar)_{max}$ previous studies[c] |
|---|---|---|---|---|---|---|---|---|
| MORB glasses: | | | | | | | | |
| 2ΠD43 sth[d] | 234.8 | 3510 | 22 | 6301 | 87.0 | 2138 ± 65 | 29400 ± 850 | n.d.[e] |
| 2ΠD43 cr[d] | 78.8 | 3510 | 10 | 4624 | 87.3 | 2173 ± 67 | 26600 ± 1080 | 27900 ± 1500 |
| 2ΠD40 sth | 374.4 | 4620 | 16 | 191 | 99.6 | 22180 ± 1630 | 27800 ± 1220 | 28150 ± 330 |
| CYP7806-11 sth | 586.8 | 2580 | 20 | 156 | 97.4 | 8324 ± 757 | 20800 ± 410 | 15560 ± 1400<br>16770 ± 3400 |
| CYP7806-11 cr#1+2[f] | 295.0 | 2580 | 12 | 82 | 97.5 | 8452 ± 198 | 19800 ± 2370 | n.d. |
| CYP7806-11 cr #1 | (~100) | | 8 | 36.1 | 95.3 | 5266 | 17000 ± 2170 | |
| CYP7806-11 cr #2 | (~200) | | 4 | 45.9 | 99.1 | 15941 | 19800 ± 2370 | |
| 2ΠD44 sth | 470.7 | 3290 | 20 | 97.8 | 26.0 | 398 ± 23 | 12500 ± 1360 | 4995 ± 90 |
| 2ΠD44 cr | 342.6 | 3290 | 5 | 12.1 | 71.8 | 1022 ± 20 | 8880 ± 1060 | n.d. |
| Loihi seamount glasses: | | | | | | | | |
| S2335-6 sth | 461.7 | 4983 | 15 | 10.88 | 90 | 2190 ± 150 | 6590 ± 840 | 4256 ± 123 |
| S2335-6 cr | 134.5 | 4983 | 5 | 1.90 | 95 | 3391 ± 849 | 7460 ± 3130 | 1249 ± 21 |
| S2335-10 sth | 382.6 | 5000 | 14 | 8.96 | 84 | 1542 ± 122 | 4380 ± 1320 | 6307 ± 356 |
| S2335-10 cr | 288.7 | 5000 | 4 | 0.28 | 42 | 493 ± 55 | 1360 ± 715 | n.d. |
| S2341-2 sth | 207.1 | 2943 | 14 | 132.3 | 5.5 | 312 ± 2 | 2490 ± 365 | 364 ± 6 |
| S2341-2 cr | 205.9 | 2943 | 7 | 112.1 | 3.9 | 307 ± 1 | 5970 ± 1960 | n.d. |

[a] Eruption depth from Staudacher et al. (1989) and Valbracht et al. (1997).
[b] For calculation of mantle argon, see text.
[c] Sarda et al. (1985), Staudacher et al. (1989), Valbracht et al. (1997), and Moreira et al. (1998).
[d] sth: stepheating; cr: crush.
[e] n.d.: not determined.
[f] Two fragments (#1 and #2) of CYP7806-11 were crushed subsequently; elemental concentrations refer to total weight of 295.0 mg.

mass spectrometric analyses. However, the contribution of such vesicles was considerable minor.

$^{40}Ar$-$^{39}Ar$ analysis followed standard procedures given by Jessberger et al. (1980). The samples were wrapped in Al foil (99.999% purity) and stacked in a quartz ampoule that was evacuated afterwards. As MORB glasses are typically depleted in mantle-derived $^{36}Ar$, we chose a short irradiation time of 24 h at the GKSS reactor in Geesthacht, Germany, yielding a relatively low neutron flux to minimize neutron-induced $^{36}Ar$ production by the $^{40}Ca(n, n\alpha)^{36}Ar$ reaction. As typical K and Ca concentrations in MORB are 400 to 2500 ppm K and 7 to 9% Ca (Basaltic Volcanism Study Project, 1981; Sarda et al., 1985), this flux was high enough to produce measurable amounts of $^{39}Ar$ and $^{37}Ar$ from K and Ca, the anticipated tracers for glass matrix diffusion. However, Cl concentrations can be much lower, ranging down to ~20 ppm (Michael and Schilling, 1989). As the $^{37}Cl(n,\gamma\beta^-)^{38}Ar$ reaction is driven by thermal neutrons as well, we omitted the cadmium shielding that was used previously to prevent irradiation damage by suppressing the thermal neutron flux. This measure enhanced $^{38}Ar$ production from Cl by a factor of 30, sufficient to allow accurate measurements of Cl. Irradiation damage was found to change Ar release properties at a fast neutron fluence of $20 \times 10^{18}$ $n_f/cm^2$ (Horn et al., 1974) but not for $2 \times 10^{18}$ $n_f/cm^2$. For a submarine basalt glass, Stettler and Bochsler (1979) reported uptake of atmospheric $^{36}Ar$ in samples irradiated with 3.0 and $5.6 \times 10^{18}$ $n_f/cm^2$ but not with $0.4 \times 10^{18}$ $n_f/cm^2$. The fast neutron flux used in this study was $0.09 \times 10^{18}$ $n_f/cm^2$; the total flux (i.e., including thermal neutrons) was $3.1 \times 10^{18}$ $n/cm^2$. In all the samples investigated here, we could not observe enhanced concentration of atmospheric Ar when compared to the unirradiated samples analysed previously (Sarda et al., 1985; Staudacher et al., 1989; Valbracht et al., 1997; Moreira et al., 1998). Apparently, irradiation damage did not induce additional incorporation of atmospheric argon for our samples, most probably because thermal neutrons deposit orders of magnitude less energy (and irradiation damage) than fast neutrons. Stettler and Bochsler (1979) considered another effect as being due to neutron irradiation, i.e., a redistribution of excess (mantle) $^{40}Ar$ from high-temperature release sites (> 900 °C) into low-temperature release sites. However, we can safely exclude such an effect for the samples studied here: Some (e.g., 2ΠD40, S2335-10) release mantle argon exclusively at high temperatures, demonstrating that the low neutron fluence applied to our samples caused not even minor redistribution of mantle argon. In fact, release of mantle argon at low temperatures is related to vesicularity as shown below.

The J- value was $(3.78 \pm 0.04) \times 10^{-4}$, as determined by NL25 hornblende flux monitors (Schaeffer and Schaeffer, 1977). Correction factors for interfering isotopes determined by $CaF_2$ monitors were $(^{36}Ar/^{37}Ar)_{Ca} = (4.21 \pm 0.41) \times 10^{-4}$, $(^{38}Ar/^{37}Ar)_{Ca} = (3.27 \pm 0.31) \times 10^{-4}$, $(^{39}Ar/^{37}Ar)_{Ca} = (9.13 \pm 0.65) \times 10^{-4}$. $(^{38}Ar/^{39}Ar)_K = (2.0 \pm 0.5) \times 10^{-2}$ was taken as average from previous Cd-shielded irradiations, $(^{40}Ar/^{37}Ar)_{Ca} = (3\pm3) \times 10^{-3}$ by Turner, 1971; $(^{40}Ar/^{39}Ar)_K = (1.23 \pm 0.24) \times 10^{-2}$ by Brereton, 1970. Although the latter correction factor might have been changed due to renouncing the Cd shielding, even application of the most extreme value of $30 \times 10^{-2}$ compiled by McDougall and Harrison (1999) does not change our basic conclusions: Maximum $^{40}Ar/^{36}Ar$ ratios (Table 1) constraining mantle source compositions would be affected by less than permil corrections, and glass-dissolved mantle argon of highly vesicular samples would be overestimated (see footnote c in Table 2).

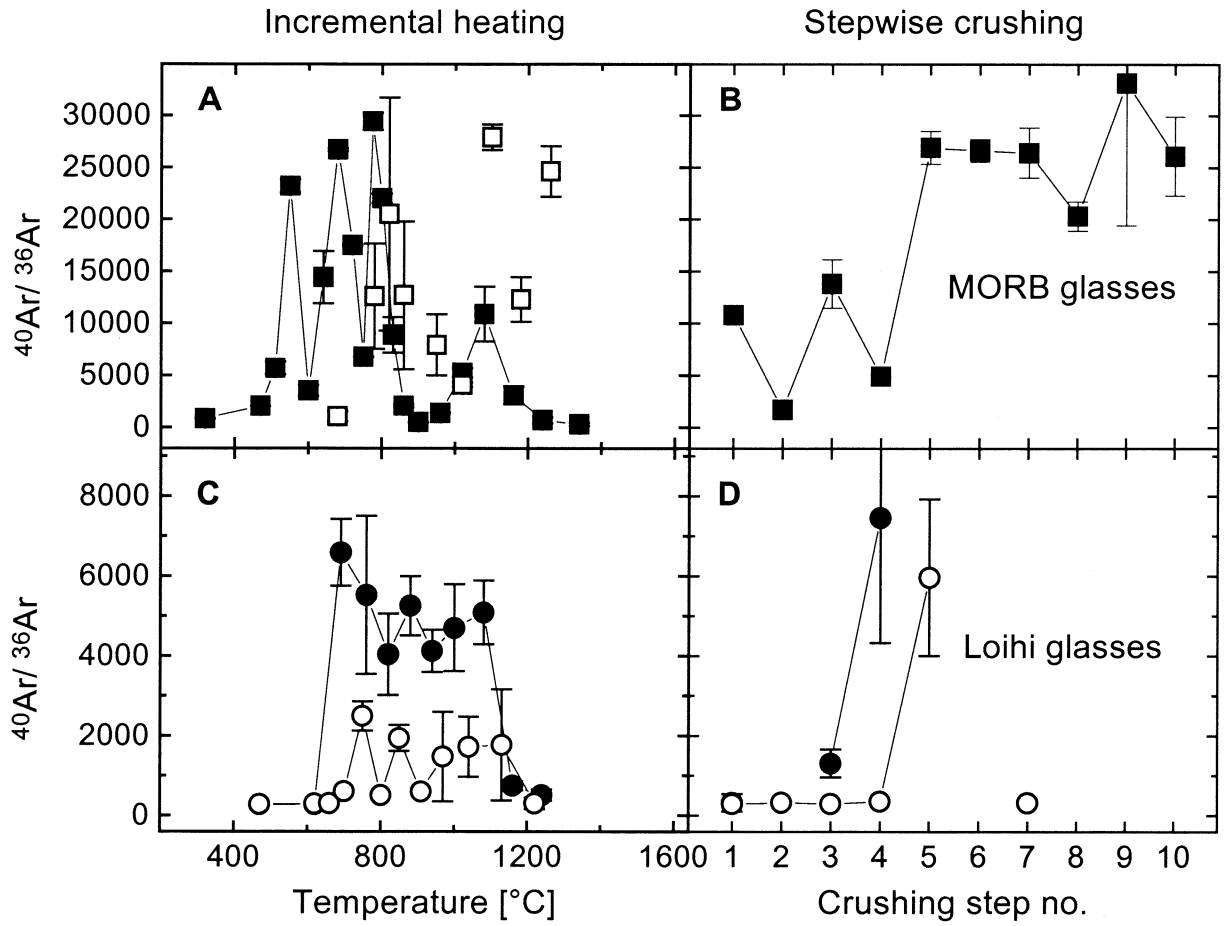


Fig. 3. The isotopic composition of Ar obtained by stepheating and stepcrushing of the vesicle-rich glasses popping rock 2ΠD43 (solid squares), S2341-2 (open circles), and the low-vesicularity glasses 2ΠD40 (open squares) and S2335-6 (solid circles).

After irradiation and before transfer into the extraction line, the glassy samples were unwrapped to avoid minuscule contributions of atmospheric argon possibly associated with the Al foil. The glass samples were stepwise heated to temperatures from 300 to 1550 °C using an induction-heated furnace with $^{40}$Ar blank values of 0.014 to 0.034 at 1000 °C and 0.13 to 0.26 at 1400°C ($\times$ $10^{-8}$ccSTP, 10-min heating duration). Each sample was heated in a final step at 1530 °C but only listed in the Appendix tables if at least one isotope was significantly different from zero. The near zero concentrations in the final high-temperature extractions indicate that all samples were totally degassed. Crushing was performed using a static pressure fracturing device developed by Jessberger and Gentner (1972). Crusher blanks were 0.008 to 0.012 $\times$ $10^{-8}$ccSTP$^{40}$Ar. Apparent ages in Appendix tables were calculated using the Steiger and Jäger (1977) conventions. Mass spectrometric analyses followed procedures described by Jessberger et al. (1980). In our study, we also addressed a potentially fundamental problem in analysing mantle argon with high $^{40}$Ar/$^{36}$Ar ratios. Many high $^{40}$Ar/$^{36}$Ar ratios reported previously were calculated after substantial (i.e., $>$ 50%) blank corrections of $^{36}$Ar. In such cases, it is of crucial importance to precisely measure system blanks and to consider possible systematic uncertainties. One such source of systematic uncertainty is a possible change of sensitivity (and mass discrimination) with partial pressure in the mass spectrometer (Burnard and Farley, 2000). This effect cannot be monitored by regularly measuring a standard air volume (measured always at the same partial pressure) but requires the analysis of fractions and multiples of the standard volumes. For example, if a sample extraction with $^{40}$Ar/$^{36}$Ar = 20,000 is corrected for 50% $^{36}$Ar blank contribution (yielding a blank-corrected $^{40}$Ar/$^{36}$Ar ratio of $\sim$40,000), blank and sample are measured at partial pressures differing by a factor of 100. In Heidelberg, we typically observe a 10 to 15% decrease in sensitivity with an increase in partial pressure by two orders of magnitude. Hence, if this effect is not considered, blank-corrected $^{40}$Ar/$^{36}$Ar ratios could be systematically overestimated by $\sim$10 to 15%. Completing these considerations, we note that in Heidelberg we have regularly monitored and corrected for this effect since 1992 (e.g., Trieloff et al., 1997), and appropriate corrections have also been made for data presented here, although blank corrections were generally not substantial, in particular, for the highest $^{40}$Ar/$^{36}$Ar ratios obtained.

## 3. PARTITIONING OF MANTLE Ar AND ATMOSPHERIC Ar BETWEEN VESICLES AND MATRIX OF SUBMARINE BASALT GLASS

We analysed four MORB and three Loihi glasses by stepwise argon extraction with up to 12 crushing and 22 heating steps per sample. Detailed data tables are given in the Appendix with a summary for each sample in Table 1. Maximum $^{40}Ar/^{36}Ar$ ratios obtained for single samples by our high-resolution analyses exceed previously determined values in most cases or include overall maximum values for MORB and Loihi samples close to $^{40}Ar/^{36}Ar$ of ~30,000 or 8000, respectively (Table 1). Very high and low $^{40}Ar/^{36}Ar$ ratios occur in both stepheating and stepcrushing experiments. Before discussing the natural (mantle and atmospheric) argon isotopes, we will consider the neutron-induced isotopes (Fig. 2).

### 3.1. Neutron-Induced Argon Isotopes

From the total concentration of neutron-induced $^{39}Ar$,$^{37}Ar$, and $^{38}Ar$, we could infer bulk concentrations of 300 to 5000 ppm K, 5 to 7% Ca, and 20 to 400 ppm Cl for the MORB glasses that are in good agreement with typical MORB glass values (e.g., Basaltic Volcanism Project, 1981). Checking the glass thin sections by SEM, we found that the glasses were largely homogeneous except for rare crystallization seeds.

Figure 2A,B displays the release pattern of neutron-induced argon isotopes for MORB glasses 2ΠD43 and 2ΠD40. It can be verified that all neutron-induced isotopes are released indistinguishably, although the specific release patterns vary from sample to sample, with release temperatures between 800 and 1300 °C. Nevertheless, a two-peaked release pattern is common to all MORB glass samples. It is highly unlikely that one of the release peaks can be ascribed to degassing of a minor phase, as such a phase would have to contain about half of the bulk Ca, K, and Cl and, hence, should be highly (and equally) enriched in these elements whereas the glass would be correspondingly depleted by a factor of two, which is particularly improbable for the major element Ca. We can conclude that most of the neutron-induced argon isotopes are distributed homogeneously in the glass matrix, but it is difficult to explain why they are released in two separate peaks. It should be noted that the release pattern cannot be attributed to the atomic sites of the respective ions, as $^{37}Ar$ from Ca and $^{39}Ar$ from K are displaced by 0.3 and 0.1 $\mu$m, i.e., several thousand atomic distances, due to recoil against the proton and alpha particle leaving the nuclei (Turner and Cadogan, 1974; Huneke and Smith 1976). This process should lead to a random distribution of the neutron-induced argon atoms, similar to naturally dissolved argon atoms, and supports our approach tracing glass dissolved via neutron-induced argon. We also can exclude that the two-peaked release pattern is an artifact of neutron irradiation (e.g., radiation damage), as non-irradiated subsamples of these glasses also yielded a two-peaked release pattern for magmatic $CO_2$ and $^4He$ (Thermoanalyzer studies at University of Jena, K. Heide, pers. comm.). However, these studies have shown preferential release of $H_2O$ in the first and $SO_2$ in the second release peak, indicating that volatile release is triggered by physicochemical processes remaining to be studied.

Figure 2C,D shows a similar two-peaked release pattern for Loihi glasses, however with one notable exception: In all three Loihi glasses (for S2335-10, see Appendix Table A10), there is an additional $^{37}Ar$ release at high temperatures of ~1300 °C. The release peak at such temperatures is a characteristic feature of Ca-rich pyroxene (e.g., Trieloff et al., 1997, and references therein) and quite certainly can be ascribed to pyroxene phenocrysts or microlites.

### 3.2. Natural Argon Isotopes

Figure 3B shows the isotopic composition of Ar extracted by crushing from popping rock 2ΠD43 in 10 steps: The $^{40}Ar/^{36}Ar$ ratios cover the range between the atmospheric value (295.5) and ~30,000 in advanced crushing steps. This indicates that some vesicle populations are severely contaminated by atmospheric Ar, while others remain largely uncontaminated, which is in agreement with results by Burnard et al. (1997), Moreira et al. (1998), and Fisher (1994). Taking a value of $^{40}Ar/^{36}Ar = 30{,}000$ as a minimum value for Ar in the upper mantle (cf. below), we calculate the release patterns in the stepheating experiment of both mantle-derived (stars in Fig. 4A) and atmospheric Ar (solid triangles in Fig. 4A) by using:

$$F(^{40}Ar_{mantle}) = [(^{36}Ar/^{40}Ar)_{sample} - (^{36}Ar/^{40}Ar)_{atm}]/[(^{36}Ar/^{40}Ar)_{mantle} - (^{36}Ar/^{40}Ar)_{atm}]$$

where F is the fraction of mantle $^{40}Ar$ (note that the results are rather insensitive to the exact mantle endmember $^{40}Ar/^{36}Ar$ value used; it may be 30,000 or 40,000). With the exception of the first two stepheating extractions of 2ΠD43, atmospheric Ar is significant at ~900 °C, whereas mantle Ar dominates the 600 to 800 °C range. For comparison, in Figure 4A the release pattern of the neutron-induced Ar isotopes (from Fig. 2) is given as open circles. It can be verified that mantle and atmospheric Ar are not released in correlation with neutron-induced argon isotopes and, hence, are only to a very small extent related to the volume of the glass. This can be quantified in Table 2 (columns 4 and 8), where we calculated the maximum possible Ar fraction that correlates exactly 1:1 with the glass component. It is simply given by the minimum ratio of the mantle or atmospheric component vs. the neutron-induced (glass-dissolved) component in any of the extraction steps of the glass release regime. For 2ΠD43, < 1% atmospheric or mantle argon can be dissolved homogeneously in the glass. Indeed, our crushing experiments extracted more than 70% of the total argon (Table 2, columns 3 and 7), indicating that most Ar resides within vesicles.

For low-vesicularity MORB glass 2ΠD40, the isotopic variations (Fig. 3A) and the Ar release patterns (Fig. 4B) are quite different: ~60% of mantle-derived Ar is degassed together with neutron-induced isotopes from the volume of the glass (Table 2, column 4) between 1000 and 1300 °C, where highest $^{40}Ar/^{36}Ar$ ratios close to 30,000 were obtained. Such a trend of increasing fraction of mantle Ar that is dissolved in the glass with decreasing vesicularity also holds for the other MORB samples with intermediate vesicularity (Table 2, column 4) and for the Loihi glasses (Table 2; Figs. 3C,D, 4C,D). That trend is expected from the low solubility of argon in silicate melts; melt-gas partitioning follows Henry's law with an average Henry constant of $\sim 8 \times 10^{-5}$ ccSTP/g bar from low pressures of 1 bar (overview in Ozima and Podosek, 2002 or, e.g.,

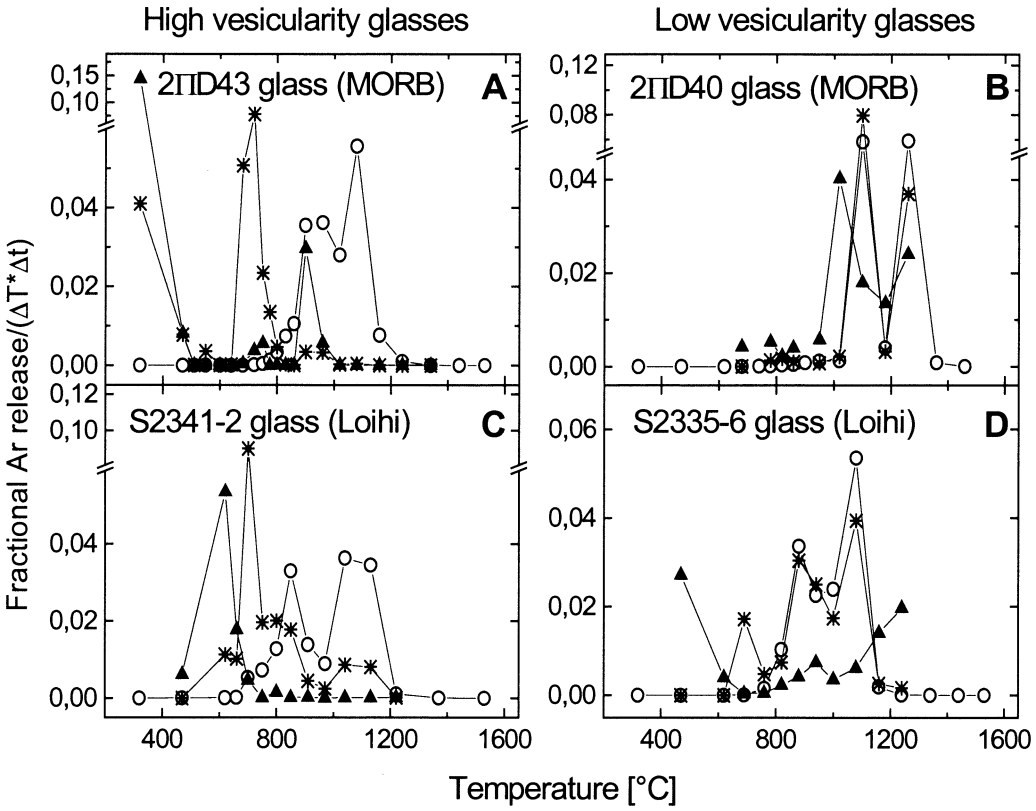


Fig. 4. Fractional Ar release vs. temperature for stepwise heating experiments. Neutron-induced Ar isotopes (open circles) represent release of Ar homogeneously dissolved in the glass matrix. Mantle-derived Ar (stars) is well correlated with glass-dissolved Ar in glasses 2ΠD40 and S2335-6 with low vesicularities on the order of permil. In glasses with vesicularity of > 1% (2ΠD43, S2341-2), a higher proportion of mantle-derived Ar is released below 800 °C from decrepitating vesicle populations. Most of the atmospheric Ar (solid triangles) is uncorrelated to glass-dissolved Ar.

Kirsten, 1968; Jambon et al., 1985; Broadhurst et al., 1992) up to high pressures of 1.1 kbar (Shibata et al., 1994) and 50 kbar (Schmidt and Keppler, 2002). To quantitatively check if argon distribution between vesicles and glass in our samples follows predicted equilibrium solubilities, we calculated the argon partial pressure in vesicles (Table 2, column 5) for a glass density of 3 g/cc and an equilibrium temperature of 1100 °C (the position of the high-temperature release peak of the glass-dissolved argon isotopes). Inferred Henry constants (Table 2, column 6) agree surprisingly well with the experimentally determined values, taking into account that only upper limits could be determined for Loihi glass vesicularities (and Henry constants). We also note that the total vesicle pressure can be roughly estimated assuming $CO_2/^{40}Ar = 30{,}000$ (Burnard et al., 1997), resulting in a few hundred bars for 2ΠD43 and 2ΠD40 (for 1100 °C), which is in good agreement with the hydrostatic pressure (~1 bar/10-m water depth) of a few hundred bars in a few km depth. We conclude that the distribution of mantle argon between glass and vesicles is governed by melt-gas equilibration upon eruption and quenching under high hydrostatic pressure, which is in agreement with experimentally determined values for the Henry constant. In stepheating experiments, mantle argon from vesicles is mostly released between 600 and 900 °C, whereas glass-dissolved mantle argon is released between 800 and 1300 °C.

Remarkably, atmospheric Ar in none of our samples—neither high nor low vesicularity glasses—really correlates with neutron-induced Ar (Fig. 4; Table 2, column 8). Generally < 30% of $Ar_{atm}$ can be homogeneously dissolved in the glass, and up to 86% is present in vesicles opened by crushing (Table 2, column 7). This new result challenges previous models that atmospheric noble gases are dissolved in the glass (Marty et al., 1983; Jambon et al., 1985; Marty and Ozima, 1986). By contrast, our results rather indicate a higher concentration of crush-related atmospheric argon (Table 2, column 9) with increasing vesicularity, which is in line with conclusions by Ballentine and Barfod (2000) that atmospheric contamination is somehow associated with vesicles, possibly secondary microfractures, microvesicles, or some original vesicles that were opened after sampling, equilibrated with air, and resealed. In column 12 of Table 2 we calculated the required fraction of vesicles filled with 1-bar air to account for all crush-released atmospheric argon of each of the samples. It can be shown that only a very small fraction of the sample's vesicles need to be contaminated to explain vesicle-related atmospheric argon: ~3% for highly vesicular samples, < 1% for low vesicular samples, due to the relatively high abundance of argon in air (0.93% vs. 0.03‰ in mantle $CO_2$ gas).

However, our results also point to other carrier phases of contaminating atmospheric argon: In the case of the Loihi

Table 2. Distribution of mantle and atmospheric Ar between glass, vesicles, and other phases.

| Glasses | Vesicularity [%][a] | $^{40}Ar_{mantle}$ crush[b]/ stepheat [%] | $^{40}Ar_{mantle}$ glass[b,c]/ total [%] | $^{40}Ar_{mantle}$ vesicle pressure[d] (1100 °C) [bar] | Henry constant[d] [$10^{-5}$ ccSTP $^{40}Ar_{mantle}$/g bar] | $^{40}Ar_{atm}$ crush[b]/ stepheat [%] | $^{40}Ar_{atm}$ glass[b,c]/ total [%] | $^{40}Ar_{atm}$ crush [$10^{-8}$ ccSTP/g] | $^{40}Ar_{atm}$ glass [$10^{-8}$ ccSTP/g] | $^{40}Ar_{atm}$ remaining [$10^{-8}$ ccSTP/g] | Fraction of vesicles with 1 bar air[e] [%] |
|---|---|---|---|---|---|---|---|---|---|---|---|
| MORB glasses | | | | | | | | | | | |
| 2ΠD43 | 7.8 ± 1.0 | 74 | 0.71 | $5.9 \times 10^{-3}$ | 6.6 | 72 | 0.08 | 590 | 0.66 | 229 | 2.43 |
| 2ΠD40[f] | 0.04 ± 0.02 | 40[f] | 60 | $2.1 \times 10^{-2}$[f] | 5.3[f] | <69[f] | 31 | <0.53[f] | 0.24 | <0.53[f] | <0.37[f] |
| CYP7806-11 | 0.76 | 52 | 7.2 | $1.2 \times 10^{-3}$ | 9.3 | 52 | 20.8 | 2.11 | 0.84 | 1.10 | 0.09 |
| 2ΠD44 | 1.0 ± 0.1 | 34 | 9.9 | $9.7 \times 10^{-5}$ | 26 | 4.7 | 0.7 | 3.40 | 0.51 | 68.5 | 0.11 |
| Loihi glasses | | | | | | | | | | | |
| S2335-6 | <0.29 | 18.3 | 69.6 | $>7.0 \times 10^{-5}$ | <98 | 8.4 | 11.0 | 0.09 | 0.12 | 0.88 | >0.01 |
| S2335-6[g] | | 8.3 ± 0.8 | | | | 2.3/9.0 | | | | | |
| S2335-10 | <0.15 | 1.6 | 99.9 | $>9.0 \times 10^{-6}$ | <832 | 11.4 | 13.3 | 0.16 | 0.19 | 1.08 | >0.03 |
| S2341-2 | 1.14 ± 0.1 | 60 | 23.8 | $4.3 \times 10^{-5}$ | 40 | 86 | 0.022 | 108 | 0.03 | 17.5 | 3.03 |

[a] Obtained by petrographic point counting.

[b] Ar released by crushing and Ar homogeneously dissolved in the glass (columns 3+4 and 7+8) is generally <100%, possibly due to (1) sample inhomogeneities (2) incomplete crushing (3) other phases hosting Ar, e.g., microdefects or heterogeneous Ar distribution in the glass.

[c] Ar correlating exactly 1:1 with the glass component. It was calculated from the *minimum ratio* of the mantle or atmospheric component vs. the glass-dissolved component in any of the extraction steps of the glass release regime. For mantle/atmospheric Ar, minimum ratios were used from 1160/1040 °C (2ΠD43), 1200/1060 °C (2ΠD40), 1220/1060 °C (CYP7806-11), 1190/1140 °C (2ΠD44), 1000/1080 °C (S2335-6), 1140/1060 °C (S2335-10), and 1040/1040 °C (S2341-2) temperature steps. Application of an extreme ($^{40}Ar/^{39}Ar)_K$ correction factor of $30 \times 10^{-2}$ (see experimental procedures) would mainly result in a lower glass-dissolved mantle argon component, most severely affected would be 2ΠD44 (8.7% instead of 9.9%) and S2341-2 (16% instead of 23.8%).

[d] Vesicle pressure calculated from mantle argon released by crushing, vesicularity, glass density of 3 g/cc, for 1100 °C (high temperature release peak of glass-dissolved argon). Henry constant calculated from vesicle pressure and glass-dissolved argon component (correlating with neutron-induced argon isotopes).

[e] Assuming that atmospheric argon extracted by crushing was released from (resealed) vesicles that equilibrated with 1 bar air (0.93% Ar).

[f] As no crushing data were available, value of non glass dissolved argon was taken, actually an upper limit for crush yield and vesicle pressure, and lower limit for the Henry constant.

[g] Sample analysed by Valbracht et al. (1997).

glasses S2335-6 and S2335-10, > 75% of the atmospheric argon detected was neither released by crushing nor related to glass-dissolved argon isotopes. However, it can be verified from Figure 4D (for S2335-6, but the same holds for S2335-10; see Appendix Table A10) that a major part of atmospheric argon is released at 1200 to 1300 °C, i.e., coincident with release of $^{37}Ar$ from pyroxene microlites (Fig. 2C,D). Release at such high temperatures—clearly after all argon had been released from the glass—makes us conclude that this contamination is related to the pyroxene lattice, which is most probably easier to achieve by contamination upon eruption and subsequent quenching and recrystallization. In the case of MORB glass 2ΠD44, ~95% of the total atmospheric argon is released in the single extraction at 930 °C (Appendix Table A6). As it is not associated with a concomitant increase in neutron-induced argon isotopes, it is most probably bound to a minor phase that does not remarkably influence the Ca, K, Cl budget. However, this particular phase is not very well constrained, and its low decomposition temperature slightly above 900 °C. In this respect we note that it can be inferred from 2ΠD44 data by Staudacher et al. (1989) that this glass contains highly fractionated atmospheric noble gases with $^{36}Ar/^{22}Ne$ ranging between 0.1 and 34 (unfractionated air: 18.8). Such fractionated atmosphere-derived contaminants with both higher and lower than atmospheric $^{36}Ar/^{22}Ne$ have also been identified by Trieloff et al. (2002) and Althaus et al. (2003).

## 4. THE ISOTOPIC COMPOSITION OF Ar IN THE EARTH'S MANTLE

### 4.1. Ar in the Depleted Upper Mantle

To reveal the isotopic composition of upper mantle argon, the highest measured $^{40}Ar/^{36}Ar$ ratios must principally be considered as lower limits because removal of atmospheric contamination may still have been incomplete. However, the definition of a single "highest value" is not an easy task, as it must take into account individual uncertainties, statistical effects, and possible sources of systematic errors (see "Samples and Experimental Procedures"). For example, Trieloff et al. (2001) have argued that due to limited analytical precision and associated statistical effects, repeated measurements of any value inevitably yield single measurements that are even higher than the true value plus the $1\sigma$ uncertainty (e.g., in a gaussian distribution, 17% of the values). It is most probably that the highest ever measured $^{40}Ar/^{36}Ar$ ratios belong to that kind. To minimize that statistical effect, we use lower isotopic composition limits defined by the individual $2\sigma$ uncertainties in the following discussion.

The highest $^{40}Ar/^{36}Ar$ ratio encountered in our study is 29,400 ± 850 from the 775 °C extraction fraction of popping rock 2ΠD43 (Table 1). The lower limit, >27,700 at the $2\sigma$ level, represents the most stringent limit ever obtained by stepheating or crushing MORB glasses. This high ratio results from a high-resolution degassing experiment with 22 instead of

the usual few extraction steps. In such an experiment, a better separation of the Ar components, and thus a better definition of their isotopic compositions, is expected. A similar result was obtained for the low-vesicularity glass 2ΠD40 (27,800 ± 1220, this work; 28,150 ± 330, Staudacher et al., 1989), setting a lower limit of > 27,490 at the 2$\sigma$ level. Regarding the conclusions by Ballentine and Barfod (2000) and this study that the degree of atmospheric contamination is correlated with vesicularity, the low-vesicular glass 2ΠD40 should be affected by only minor contamination and provide a maximum $^{40}Ar/^{36}Ar$ ratio close to the mantle source value. This conclusion is also supported by considering the improvements of maximum $^{40}Ar/^{36}Ar$ ratios obtained in previous low-resolution experiments (Table 1). For strongly contaminated samples like 2ΠD44, we could improve the maximum $^{40}Ar/^{36}Ar$ value from 5000 to 12,500, i.e., by 150%, and for the intermediate contaminated sample, CYP7806-11, from 16,000 to 21,000 (~30%). However, for samples 2ΠD43 and 2ΠD40, with previously determined maximum $^{40}Ar/^{36}Ar$ ratios close to 30,000, our improvements were hardly significant, indicating that a limiting value is approached. A similar lower limit can be inferred from a laser extraction study of 2ΠD43 with high spatial resolution by opening single vesicles (Burnard et al., 1997): The maximum value of 40,000 ± 4000 defines a lower limit of > 32,000 at the 2$\sigma$ level. However, the latter value is more susceptible to systematic uncertainties associated with $^{36}Ar$ blank corrections (see "Samples and Experimental Procedures") that were much higher (~50%) than for the maximum stepheating value obtained in this study on 2ΠD43 (~1%).

Another commonly used tool to discriminate against atmospheric contamination is plotting $^{40}Ar/^{36}Ar$ vs. $1/^{36}Ar$ (Ozima and Podosek, 2002). Figure 5 displays Ar data of popping rock 2ΠD43 obtained in three different laboratories with different extraction techniques: Laser-induced vesicle decrepitation (Fig. 5A: Manchester university, Burnard et al., 1997), pressure fracturing (Fig. 5B: Heidelberg university, this study), and ball-mill crushing (Fig. 5C: IPG Paris, Staudacher et al., 1989; Moreira et al., 1998; Kunz, 1999). All three studies yield (1) steep mixing arrays between an atmospheric and a mantle component with high $^{40}Ar/^{36}Ar$ ratios (open squares) and (2) horizontal trends (solid squares) indicating an endmember with only minor contamination effects. Average values of these horizontal trends are 32,400 ± 4200 (Fig. 5A), 27,800 ± 3000 (Fig. 5B), and 23,700 ± 2300 (Fig. 5C). The value defined by the Manchester data ($^{40}Ar/^{36}Ar$ = 32,400 ± 4200) can be reconciled with the 2$\sigma$ lower limits of the 2ΠD43 maximum values obtained in Heidelberg (29,400 ± 850), Paris (27,900 ± 1500), Manchester (40,000 ± 4000), or maximum values obtained on other MORB samples in previous studies (Sarda et al., 1985; Staudacher et al., 1989; Fisher, 1994). Hence, a value of 32,000 ± 4000 seems to us the most reasonable and conservative estimate for upper mantle argon, taking into account all available data.

### 4.2. Ar in the Loihi Mantle Plume Source

In our study of Loihi glass, we measured the highest $^{40}Ar/^{36}Ar$ ratio, 6590 ± 840, in the 690 °C extraction fraction of S2335-6 (Table 1, Fig. 3C). From the degassing pattern (Fig. 4D), we can infer that this Ar resides in the few vesicles of this low-vesicularity glass, since it is not accompanied by neutron-induced, i.e., glass-dissolved, Ar. Similarly high $^{40}Ar/^{36}Ar$ ratios, but with relatively large uncertainties, are observed in some crushing steps of S2335-6 and S2341-2 (Fig. 1D) but also for the glass-dissolved component of S2335-6. Similarly to the MORB glasses, our high-resolution experiments were able to improve previously obtained maximum $^{40}Ar/^{36}Ar$ ratios for the strongly contaminated glass S2341-2: 2490 ± 365 and 5970 ± 1960 in this study (Table 1) vs. 364 ± 6 by Valbracht et al. (1997). However, for the glasses S2335-6 and S2335-10 that have high solar-like $^{20}Ne/^{22}Ne$ ratios (Fig. 1) and should be least affected by contamination effects due to their low vesicularity (Table 2; Ballentine and Barfod, 2000), improvements of the maximum $^{40}Ar/^{36}Ar$ values were hardly achieved (Table 1). Hence, we regard $^{40}Ar/^{36}Ar$ of ~7000 as the best estimate for the Loihi plume source inferred from submarine basalt glasses. This value agrees well with the mantle source estimate derived from Loihi dunites of $^{40}Ar/^{36}Ar$ = 8000 (Trieloff et al., 2000).

As listed in Table 1, Valbracht et al. (1997) already measured $^{40}Ar/^{36}Ar$ ratios as high as 6307 ± 356 in the 1500 °C extraction of basalt glass S2335-10 or comparably high values of 5222 ± 53 in phenocrysts separated from another basalt glass (S2338-2). However, Valbracht et al. (1997) estimated $^{40}Ar/^{36}Ar$ of the Loihi plume source between 2500 and 5000, as they did not ascribe the high $^{40}Ar/^{36}Ar$ ratios in the 1500 °C extractions from basalt glasses to be derived from the Loihi mantle source but to olivine phenocrysts with slightly more nucleogenic neon indicative of a MORB contamination. We do not follow this particular argument for two reasons: First, phenocryst separates analysed by Valbracht et al. (1997) with high $^{40}Ar/^{36}Ar$ ratios (from S2338-2, see above) lie left of the Loihi line in a neon three-isotope plot (e.g., Fig. 1) and, therefore, do not support "contamination" by MORB-type neon. Second, Loihi dunite xenoliths that are most probably cumulates of olivine phenocrysts have the same neon isotopic composition, i.e., no trace of MORB-like neon but $^{40}Ar/^{36}Ar$ ratios as high as 8000 (Trieloff et al., 2000).

### 4.3. Ar and Ne Isotopic Composition in the Earth's Mantle

We note here that an upper mantle $^{40}Ar/^{36}Ar$ ratio of 32,000 can be reconciled with a $^{20}Ne/^{22}Ne$ ratio of solar (implanted) Ne-B composition (12.52 ± 0.18, Black, 1972) when taking into account the $^{40}Ar/^{36}Ar$-$^{20}Ne/^{22}Ne$ correlation of 2ΠD43 (Moreira et al., 1998; Kunz, 1999; Trieloff et al., 2001) and does not require the presence of solar gas neon with $^{20}Ne/^{22}Ne$ = 13.8 (Benkert et al., 1993) in the upper mantle source (Ballentine et al., 2001). The neon isotopic composition in the Earth's mantle is of immediate importance for the accretional history of the inner solar system and Earth and for the nature of the earliest terrestrial atmosphere: $^{20}Ne/^{22}Ne$ = 12.5, i.e., Ne-B composition, would imply acquisition of solar gases by solar wind implantation into less than km-sized planetesimals during accretion and requires early dissipation of the gaseous (mainly $H_2$, He) solar nebula (Trieloff et al., 2000, 2002). $^{20}Ne/^{22}Ne$ = 13.8 would imply direct acquisition of solar gas (Pepin, 1991), possibly from a dense early protoatmosphere from which solar He and Ne dissolved into an early magma ocean (Harper and Jacobsen, 1996; Porcelli et al., 2001).

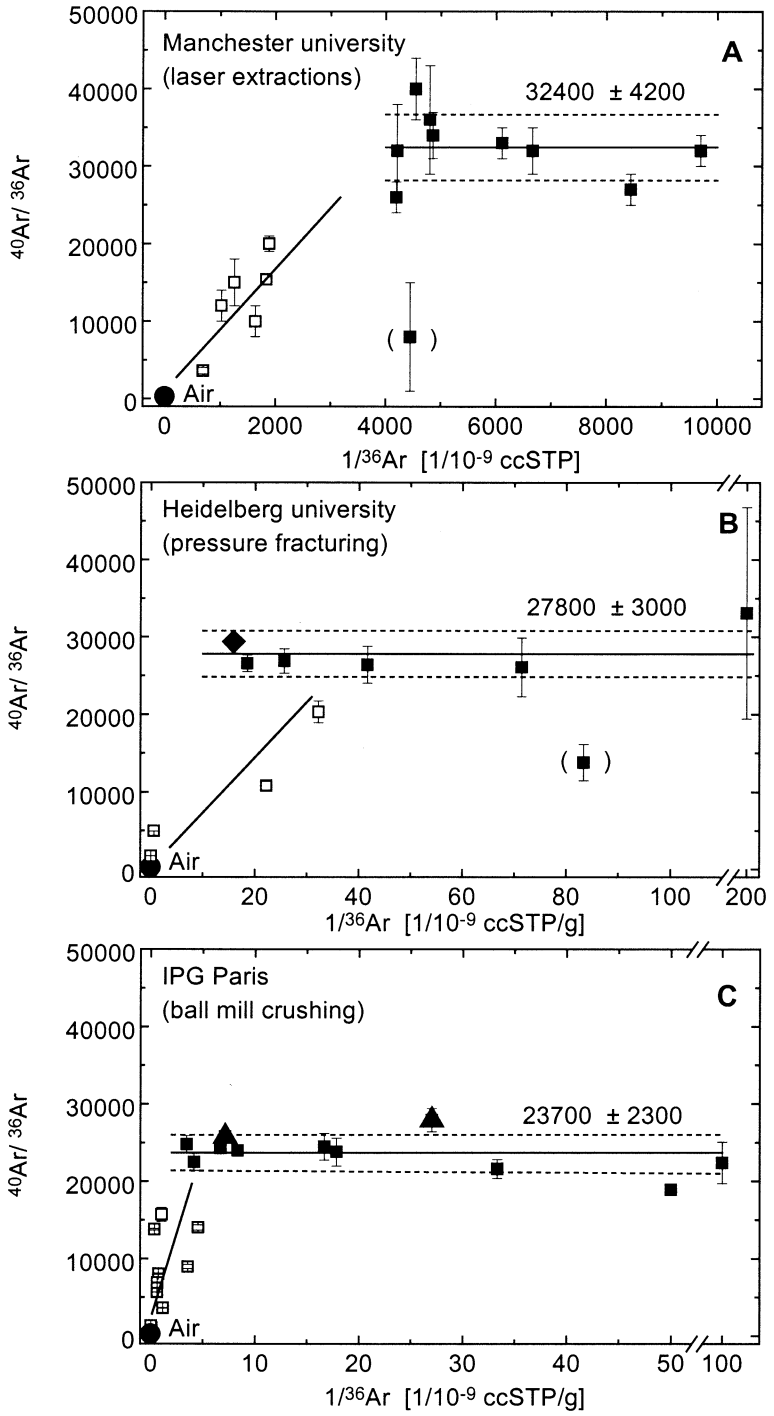


Fig. 5. $^{40}Ar/^{36}Ar$ ratio vs. inverse $^{36}Ar$ concentration of MORB popping rock 2ΠD43. (A) Laser extractions (Burnard et al., 1997). (B) Stepwise pressure fracturing (this work). (C) Stepwise ball-mill crushing (Staudacher et al., 1989, triangles; Moreira et al., 1998; Kunz, 1999). While trends (open squares) toward a y-axis intercept of 295.5 indicate local atmospheric contamination of the sample, the trends parallel to the x-axis (mean values with $1\sigma$ errors of solid square data) define mean values close to 30,000. Note that the maximum values obtained in Paris (27,900 ± 1500; Staudacher et al., 1989) and Heidelberg (29,400 ± 850, 775 °C extraction, diamond, this study) are in agreement with a value of 32,000 derived from the Manchester data (Burnard et al., 1997) and are also consistent with the highest single value of 40,000 ± 4000 at the $2\sigma$ level.

### 4.4. $^{206}Pb/^{204}Pb$-$^{40}Ar/^{36}Ar$ Correlation in MORB Glasses: Subduction of Atmospheric Argon or Severe Local Contamination of High Vesicularity Samples at Topographic Highs?

Sarda et al. (1999) suggested that a correlation of maximum $^{40}Ar/^{36}Ar$ ratios and $^{206}Pb/^{204}Pb$ ratios in mid-Atlantic ridge basalt glasses would indicate mixing between a depleted MORB endmember with high $^{40}Ar/^{36}Ar$ and low $^{206}Pb/^{204}Pb$ ratios and a recycled/subducted component with enriched $^{206}Pb/^{204}Pb$ and atmosphere-like low $^{40}Ar/^{36}Ar$. Burnard (1999) argued that the correlation has other causes: Enriched $^{206}Pb/^{204}Pb$ isotope ratios are well known to occur at topographic highs due to local plume injections. The low hydrostatic pressure at topographic highs allows vesiculation and loss of mantle volatiles as well as an increasing degree of vesicularity-related atmospheric contamination. Our results could provide a means to distinguish between these two scenarios. We found that maximum $^{40}Ar/^{36}Ar$ ratios strongly depend on the resolution, i.e., number of heating or crushing steps. Hence, experiments with even higher resolution could clarify this resolution. If upper mantle source $^{40}Ar/^{36}Ar$ ratios close to 32,000 are present in the most severely contaminated samples as well, this would favour the Burnard (1999) scenario; or if sample-specific upper limits really exist (although at a higher level than previously assumed), this would favour the subduction model of Sarda et al. (1999).

## 5. SUMMARY AND CONCLUSIONS

We performed argon analyses by both high-resolution stepheating and stepcrushing of MORB and Loihi basalt glasses that are characterised by a high variability in vesicularity (between 0.04 and 8%) and a high variability of atmospheric contamination as judged from $^{20}Ne/^{22}Ne$ ratios between the atmospheric value of 9.8 and solar-like values of $\geq$12.5. Neutron-induced argon isotopes ($^{39}Ar$ from K, $^{37}Ar$ from Ca, $^{38}Ar$ from Cl) were used to monitor release of glass-dissolved argon components during stepheating. We reached the following conclusions:

1. Glass-dissolved, neutron-induced argon isotopes are released mainly between 800 and 1300 °C in characteristic (sample-specific) two-peaked release patterns.
2. Mantle-derived argon is distributed between vesicles and glass matrix as expected from melt-gas equilibrium partitioning at eruption ($\sim$1100 °C, several 100 bars total pressure), according to Henry's law, which is compatible with experimentally determined Henry constants of $\sim(5–10) \times 10^{-5}$ccSTP $^{40}Ar_{mantle}$/g bar. This result was derived from the observation that in high-vesicularity glasses ($>$ 0.8% vesicles) most of the mantle argon is not dissolved in the glass but, instead, resides in vesicles from which it is released by crushing or stepheating between 600 and 900 °C. This had been previously recognized and is consistent with results by Marty and Ozima (1986), Jambon et al. (1985) and Staudacher et al. (1989). In low-vesicularity glasses ($<$ permil vesicularity), most mantle argon is dissolved in the glass, as inferred from the remarkable correlation with neutron-induced, glass-dissolved argon isotopes.
3. Although a significant part of atmospheric contamination is released in the same temperature range as glass-dissolved argon isotopes, only a minor fraction (generally $<$ 30%) does really correlate with neutron-induced argon isotopes. The major part is not dissolved homogeneously in the glass, which is in contrast to previous suggestions that were based on stepheating studies that did not use neutron-induced argon isotopes (Marty and Ozima, 1986; Jambon et al., 1985). On the other hand, we detected a correlation of the amount of atmospheric argon released by crushing and vesicularity, which confirms recent suggestions of association of atmospheric contamination and vesicularity (Ballentine and Barfod, 2000). If this contamination results from crush-accessible sites that equilibrated with 1-bar air, only a small fraction ($<$ 3%) of the total vesicles are needed to fully account for the observed contamination.
4. We also identified other carriers of contaminating atmospheric argon, e.g., pyroxene microlites releasing atmospheric argon at 1200 to 1300 °C during stepheating. The associated contamination process was probably different from the vesicle contamination process, perhaps occurring shortly after eruption during partial recrystallization.
5. The better resolution of our experiments, regarding the number of stepheating or stepcrushing extractions, yielded significant improvements concerning the isolation of the mantle component in strongly and intermediate contaminated MORB glass samples (2ΠD44, CYP7806-11). Previously obtained maximum $^{40}Ar/^{36}Ar$ ratios were increased up to 150%. However, for MORB samples that previously were found to have $^{40}Ar/^{36}Ar$ ratios close to 30,000, improvements were hardly significant with the most significant value being 29,400 $\pm$ 850. This effect is observed for the highly vesicular popping rock 2ΠD43 and also for the glass 2ΠD40 that has an extremely low vesicularity and, hence, a very low degree of vesicularity-related atmospheric contamination (Ballentine and Barfod, 2000). This indicates that the limiting value reached is close to the actual MORB mantle endmember composition. Similar $^{40}Ar/^{36}Ar$ plateau values emerge when considering $^{40}Ar/^{36}Ar$ vs. $1/^{36}Ar$ plots of 2ΠD43 Ar data obtained with laser extraction (Burnard et al., 1997) and pressure-fracturing techniques in this study. An upper mantle $^{40}Ar/^{36}Ar$ estimate of 32,000 $\pm$ 4000 is suggested from all available data.
6. For Loihi glasses, our experiments also yielded significantly better resolution of mantle and atmospheric argon but, again, for low-vesicularity samples that showed maximum $^{40}Ar/^{36}Ar$ ratios in previous low-resolution experiments of close to 6000 (Valbracht et al., 1997), we could hardly improve these limits; the most significant value obtained was 6590 $\pm$ 840 for sample S2335-6. This value agrees well with the Loihi mantle source estimate inferred from Loihi dunites of $^{40}Ar/^{36}Ar = 8000$ (Trieloff et al., 2000).
7. Our mantle source estimates can well be reconciled with the presence of Ne-B in Earth's mantle (Trieloff et al., 2000, 2002) and fit into the systematics that the MORB mantle excess of radiogenic nuclides is higher by about a factor of 4 to 5 than in the Loihi plume source (e.g., $[^{40}Ar/^{36}Ar_{MORB}]/[^{40}Ar/^{36}Ar_{Loihi}] = 32{,}000/8000 = 4$ or $[^{4}He/^{3}He_{MORB}]/[^{4}He/^{3}He_{Loihi}] = 90{,}000/20{,}000 = 4.5$). Such a correlation is actually expected for other reasons (Ozima and

Zahnle, 1993) and, hence, may be regarded as supporting our mantle source estimates. These estimates may be understood as an attempt to define limits that can be compellingly inferred and justified from the presently available data while acknowledging the principal possibility that not all contamination effects were fully removed. For example, while we believe that our estimates quite reliably have discriminated contamination effects by unfractionated air (related to vesicularity), more subtle "contamination" effects are possible, e.g., introduction of fractionated (Ar-rich) air possibly by subduction into both mantle reservoirs (Harrison et al., 1999, 2002; Trieloff et al., 2000, 2002). However, it must be provided that these affected both mantle sources to a similar extent, which may require very special conditions.

*Acknowledgments*—We thank T. Staudacher, P. J. Valbracht, and A. Malahoff for generous sample donations and J. Kunz, T. Staudacher, T. Althaus, and R. Altherr for helpful discussions. For careful reviews and important advice, we thank T. Hanyu, M. Moreira, and an anonymous reviewer. This work was supported by the Deutsche Forschungsgemeinschaft (grant no. TR333/2 and 3) and by A. W. Hofmann, Max-Planck-Institut für Chemie, with a MPG research stipendium.

*Associate editor:* J. -I. Matsuda

## REFERENCES

Allègre C. J., Staudacher T., and Sarda P. (1986) Rare gas systematics: Formation of the atmosphere, evolution and structure of the Earth's mantle. *Earth Planet. Sci. Lett.* **81,** 127–150.

Althaus T., Niedermann S., Erzinger J. (2003) Noble gases in olivine phenocrysts from drill core samples of the HSDP pilot and main holes. (Mauna Loa and Mauna Kea, Hawaii). *Geochem. Geophy. Geosy.* **4,** 8701.

Ballentine C. J. and Barfod D. (2000) The origin of air-like noble gases in MORB and OIB. *Earth Planet. Sci. Lett.* **180,** 39–48.

Ballentine C. J., Porcelli D., and Wieler R. (2001) Noble gases in mantle plumes. *Science* **291,** 2269a.

Basaltic Volcanism Study Project (1981) *Basaltic Volcanism on the Terrestrial Planets.* Pergamon Press, New York.

Benkert J. P., Baur H., Signer P., and Wieler R. (1993) He, Ne and Ar from the solar wind and solar energetic particles in lunar ilmenites and pyroxenes. *J. Geophys. Res.* **98,** 13147–13162.

Black D. C. (1972) On the origins of trapped helium, neon and argon isotopic variations in meteorites-II. Carbonaceous chondrites. *Geochim. Cosmochim. Acta* **36,** 377–394.

Brereton N. R. (1970) Corrections for interfering isotopes in the $^{40}$Ar-$^{39}$Ar dating method. *Earth Planet. Sci. Lett.* **8,** 427–433.

Broadhurst C. L., Drake M. J., Hagee B. E., and Bernatowicz T. J. (1992) Solubility and partitioning of Ne, Ar, Kr and Xe in minerals and synthetic basalt melts. *Geochim. Cosmochim. Acta* **56,** 709–723.

Burnard P. G. (1999) Origin of argon-lead isotopic correlation in basalts. *Science* **286,** 871a.

Burnard P. G., Farley K. A. (2000) Calibration of pressure-dependent sensitivity and discrimination in Nier-type noble gas ion sources. *Geochem. Geophy. Geosy.* **1,** 200GC000038.

Burnard P. G., Graham D., and Turner G. (1997) Vesicle-specific noble gas analyses of "popping rock:" Implications for primordial noble gases in Earth. *Science* **276,** 568–571.

Clarke W. B., Beg M. A., and Craig H. (1975) Excess $^{3}$He in the sea: Evidence for terrestrial primordial helium. *Earth Planet. Sci. Lett.* **6,** 213–220.

Craig H. and Lupton J. E. (1976) Primordial neon, helium and hydrogen in oceanic basalts. *Earth Planet. Sci. Lett.* **31,** 369–385.

Dalrymple G. B. and Moore J. G. (1968) Argon-40: Excess in submarine pillow basalts from Kilauea Volcano, Hawaii. *Science* **161,** 1132–1135.

Fisher D. E. (1971) Incorporation of Ar in East Pacific basalts. *Earth Planet. Sci. Lett.* **12,** 321–324.

Fisher D. E. (1994) Mantle and atmosphere-like argon in vesicles of MORB glasses. *Earth Planet. Sci. Lett.* **123,** 199–204.

Harper C. L. Jr. and Jacobsen S. B. (1996) Noble gases and Earth's accretion. *Science* **273,** 1814–1818.

Harrison D., Burnard P. G., and Turner G. (1999) Noble gas behaviour and composition in the mantle: Constraints from the Iceland plume. *Earth Planet. Sci. Lett.* **171,** 199–207.

Harrison D., Burnard P. G., Trieloff M., and Turner G. (in press) Resolving atmospheric contaminants in mantle noble gas analyses. Geochem. Geophy. Geosy 4, 2002GC0000325.

Hayashi C., Nakazawa K., and Mizuno H. (1979) Earth's melting due to the blanketing effect of the primordial dense atmosphere. *Earth Planet. Sci. Lett.* **43,** 22–28.

Hiyagon H., Ozima M., Marty B., Zashu S., and Sakai H. (1992) Noble gases in submarine glasses from mid-oceanic ridges and Loihi seamount: Constraints on the early history of the Earth. *Geochim. Cosmochim. Acta* **56,** 1301–1316.

Hofmann A. W. (1997) Mantle geochemistry: The message from oceanic volcanism. *Nature* **385,** 219–229.

Honda M., McDougall I., Patterson D. B., Doulgeris A., and Clague D. A. (1991) Possible solar noble-gas component in Hawaiian basalts. *Nature* **349,** 149–151.

Horn P., Jessberger E. K., Kirsten T., and Richter H. (1974) $^{39}$Ar-$^{40}$Ar dating of lunar rocks: Effects of grain size and neutron irradiation. *P. Lunar Planet. Sci. C.* **5,** 1563–1591.

Huneke J. C. and Smith S. P. (1976) The realities of recoil: $^{39}$Ar recoil out of small grains and anomalous age patterns in $^{40}$Ar-$^{39}$Ar dating. *P. Lunar Planet. Sci. C.* **7,** 1987–2008.

Jambon A., Weber H. W., and Begemann F. (1985) Helium and argon from an Atlantic MORB glass: Concentration, distribution and isotopic composition. *Earth Planet. Sci Lett.* **73,** 255–267.

Jessberger E. K. and Gentner W. (1972) Mass spectrometric analysis of gas inclusions in Muong Nong glass and Libyan Desert glass. *Earth Planet. Sci. Lett.* **14,** 221–225.

Jessberger E. K., Huneke J. C., Podosek F. A., and Wasserburg G. J. (1974) High resolution Argon analysis of neutron irradiated Apollo 16 rocks and separated minerals. *P. Lunar Planet. Sci. C.* **5,** 1419.

Jessberger E. K., Dominik B., Staudacher T., and Herzog G. F. (1980) $^{40}$Ar-$^{39}$Ar ages of Allende. *Icarus* **42,** 380–405.

Kellogg L. H., Hager B. H., and van der Hilst R. D. (1999) Compositional stratification in the deep mantle. *Science* **283,** 1881–1884.

Kirsten T. (1968) Incorporation of rare gases in solidifying enstatite melts. *J. Geophys. Res.* **73,** 2807–2810.

Kumagai H. and Kaneoka I. (1998) Variations of noble gas abundances and isotope ratios in a single MORB pillow. *Geophys. Res. Lett.* **25,** 3891–3894.

Kunz J. (1999) Is there solar argon in the Earth's mantle? *Nature* **399,** 649–650.

Kunz J., Staudacher T., and Allègre C. J. (1998) Plutonium-fission xenon found in Earth's mantle. *Science* **280,** 877–880.

Marty B. and Ozima M. (1986) Noble gas distribution in oceanic basalt glasses. *Geochim. Cosmochim. Acta* **50,** 1093–1097.

Marty B., Zashu S., and Ozima M. (1983) Two noble gas components in a Mid-Atlantic Ridge basalt. *Nature* **302,** 238–240.

McDougall I. and Harrison T. M. (1999) *Geochronology and Thermochronology by the $^{40}$Ar/$^{39}$Ar Method*, 2nd ed, Oxford University Press, New York.

Michael P. J. and Schilling J. G. (1989) Chlorine in mid-ocean ridge magmas: Evidence for assimilation of seawater-influenced components. *Geochim. Cosmochim. Acta* **53,** 3131–3143.

Moreira M., Kunz J., and Allègre C. J. (1998) Rare gas systematics in popping rock: Isotopic and elemental compositions in the upper mantle. *Science* **279,** 1178–1181.

Ozima M. (1975) Ar isotopes and Earth-atmosphere evolution models. *Geochim. Cosmochim. Acta* **39,** 1127–1134.

Ozima M. (1994) Noble gas state in the mantle. *Rev. Geophys.* **32,** 405–426.

Ozima M. and Podosek F. A. (2002) *Noble Gas Geochemistry*, 2nd ed., Cambridge University press, Cambridge.

Ozima M. and Zahnle K. (1993) Mantle degassing and atmospheric evolution: Noble gas view. *Geochem. J.* **27,** 185–200.

Patterson D. B., Honda M., and McDougall I. (1990) Atmospheric contamination: A possible source for heavy noble gases in basalts from Loihi seamount, Hawaii. *Geophys. Res. Lett.* **17,** 705–708.

Porcelli D. R. and Wasserburg G. J. (1995) Mass transfer of helium, neon, argon, and xenon through a steady-state upper mantle. *Geochim. Cosmochim. Acta* **59,** 4921–4937.

Porcelli D., Woolum D., and Cassen P. (2001) Deep Earth rare gases: Initial inventories, capture from the solar nebula, and losses during Moon formation. *Earth Planet. Sci. Lett.* **193,** 237–251.

Sarda P., Staudacher T., and Allègre C. J. (1985) $^{40}Ar/^{36}Ar$ in MORB glasses: Constraints on atmosphere and mantle evolution. *Earth Planet. Sci. Lett.* **72,** 357.

Sarda P., Staudacher T., and Allegre C. J. (1988) Ne-isotopes in submarine basalts. *Earth Planet. Sci. Lett.* **91,** 73–88.

Sarda P., Moreira M., and Staudacher T. (1999) Argon-Lead isotopic correlation in mid-Atlantic ridge basalts. *Science* **283,** 666–668.

Schaeffer G. A. and Schaeffer O. A. (1977) $^{40}Ar$-$^{39}Ar$ ages of lunar rocks. *P. Lunar Planet. Sci. C.* **8,** 2253–2300.

Schmidt B. C. and Keppler H. (2002) Experimental evidence for high noble gas solubilities in silicate melts under mantle pressures. *Earth Planet. Sci. Lett.* **195,** 277–290.

Shibata T., Takahashi E., and Ozima M. (1994) Noble gas partitioning between basaltic melt and olivine crystals at high pressures. In Noble Gas Geochemistry and Cosmochemistry (ed. J. I. Matsuda), pp. 343–354, Terra Science Publishing, Tokyo.

Staudacher T., Sarda P., Richardson S. H., Allègre C. J., Sagna I., and Dmitriev L. V. (1989) Noble gases in basalt glasses from a Mid-Atlantic Ridge topographic high at 14°N: Geodynamic consequences. *Earth Planet. Sci. Lett.* **96,** 119–133.

Steiger R. H. and Jäger E. (1977) Subcommission on Geochronology: Convention on the use of decay constants in geo- and cosmochronology. *Earth Planet. Sci. Lett.* **36,** 359–362.

Stettler A. and Bochsler P. (1979) He, Ne and Ar composition in a neutron activated sea-floor basalt glass. *Geochim. Cosmochim. Acta* **43,** 157–169.

Trieloff M., Weber H. W., Kurat G., Jessberger E. K., and Janicke J. (1997) Noble gases, their carrier phases, and Ar chronology of upper mantle rocks from Zabargad Island, Red Sea. *Geochim. Cosmochim. Acta* **61,** 5065–5088.

Trieloff M., Kunz J., Clague D. A., Harrison D., and Allègre C. J. (2000) The nature of pristine noble gases in mantle plumes. *Science* **288,** 1036–1038.

Trieloff M., Kunz J., Clague D. A., Harrison D., and Allègre C. J. (2001) Noble gases in mantle plumes. *Science* **291,** 2269a.

Trieloff M., Kunz J., and Allègre C. J. (2002) Noble gas systematics of the Réunion mantle plume source and the origin of primordial noble gases in Earth's mantle. *Earth Planet. Sci. Lett.* **200,** 297–313.

Turner G. (1971) Argon 40-argon 39 dating: The optimization of irradiation parameters. *Earth Planet. Sci. Lett.* **10,** 227–234.

Turner G. (1989) The outgassing history of the Earth's atmosphere. *J. Geol. Soc. London* **146,** 147–154.

Turner G. and Cadogan P. H. (1974) Possible effects of $^{39}Ar$ recoil in $^{40}Ar$-$^{39}Ar$ dating. *P. Lunar Planet. Sci. C.* **5,** 1601–1615.

Turner G., Burgess R., and Bannon M. (1990) Volatile-rich mantle fluids inferred from inclusions in diamond and mantle xenoliths. *Nature* **344,** 653–655.

Valbracht P. J., Staudacher T., Malahoff A., and Allègre C. J. (1997) Noble gas systematics of deep rift zone glasses from Loihi seamount, Hawaii. *Earth Planet. Sci. Lett.* **150,** 399–411.

Wetherill G. W. (1981) Solar wind origin of $^{36}Ar$ on Venus. *Icarus* **46,** 70–80.

## APPENDIX

Tables A1 to A13 display measured argon isotopes corrected for mass discrimination, sensitivity, system blanks, decay, and relative neutron doses. All isotopes are also corrected for interfering isotopes produced on K and Ca during irradiation. Remaining argon isotopes are given in ccSTP/g and have the following composition:

$$^{36}Ar = {}^{36}Ar_{man} + {}^{36}Ar_{atm}$$
$$^{37}Ar = {}^{37}Ar_{Ca}$$
$$^{38}Ar = {}^{38}Ar_{man} + {}^{38}Ar_{atm} + {}^{38}Ar_{Cl}$$
$$^{39}Ar = {}^{39}Ar_{K}$$
$$^{40}Ar = {}^{40}Ar_{man} + {}^{40}Ar_{atm}$$

Note that man = mantle-derived argon; atm = atmospheric argon; Ca = argon derived from Ca; Cl = argon derived from Cl; and K = argon derived from K.

Table A1. MOR popping rock 2ΠD43.

| Temp. [°C] | $^{36}Ar\ 10^{-12}$ | $^{37}Ar\ 10^{-12}$ | $^{38}Ar\ 10^{-12}$ | $^{39}Ar\ 10^{-12}$ | $^{40}Ar\ 10^{-9}$ |
|---|---|---|---|---|---|
| 320 | 19340 ± 810 | 0 ± 0 | 3840 ± 160 | 19 ± 4 | 16360 ± 680 |
| 470 | 3610 ± 150 | 0 ± 0 | 777 ± 33 | 28 ± 5 | 7400 ± 310 |
| 510 | 5 ± 1 | 5 ± 1 | 25 ± 1 | 3 ± 1 | 28 ± 1 |
| 550 | 34 ± 1 | 10 ± 1 | 79 ± 1 | 4 ± 1 | 784 ± 9 |
| 600 | 4 ± 1 | 15 ± 1 | 111 ± 2 | 4 ± 1 | 15 ± 1 |
| 640 | 4 ± 1 | 7 ± 1 | 14 ± 1 | 4 ± 1 | 58 ± 1 |
| 680 | 418 ± 5 | 0 ± 0 | 96 ± 3 | 36 ± 3 | 11150 ± 130 |
| 720 | 990 ± 13 | 46 ± 9 | 309 ± 8 | 74 ± 6 | 17310 ± 200 |
| 750 | 589 ± 3 | 114 ± 5 | 169 ± 2 | 24 ± 3 | 3999 ± 5 |
| 775 | 63 ± 2 | 264 ± 2 | 203 ± 2 | 42 ± 2 | 1854 ± 2 |
| 800 | 29 ± 1 | 660 ± 2 | 255 ± 1 | 106 ± 1 | 636 ± 1 |
| 830 | 5 ± 1 | 1788 ± 7 | 644 ± 3 | 278 ± 2 | 41 ± 1 |
| 860 | 9 ± 1 | 2547 ± 20 | 918 ± 7 | 355 ± 3 | 18 ± 1 |
| 900 | 3307 ± 8 | 11396 ± 29 | 4263 ± 12 | 1596 ± 8 | 1724 ± 2 |
| 960 | 991 ± 3 | 17430 ± 42 | 5723 ± 17 | 2444 ± 13 | 1362 ± 2 |
| 1020 | 22 ± 2 | 13489 ± 50 | 4290 ± 18 | 1908 ± 11 | 112 ± 1 |
| 1080 | 13 ± 3 | 26780 ± 160 | 9329 ± 59 | 4142 ± 31 | 132 ± 1 |
| 1160 | 7 ± 2 | 4930 ± 120 | 1531 ± 36 | 680 ± 16 | 23 ± 1 |
| 1240 | 7 ± 3 | 660 ± 110 | 212 ± 34 | 100 ± 16 | 5 ± 1 |
| 1340 | 13 ± 8 | 26 ± 11 | 9 ± 4 | 5 ± 2 | 4 ± 2 |
| 1440 | 6 ± 6 | 0 ± 0 | 1 ± 1 | 0 ± 0 | 3 ± 3 |
| 1530 | 6 ± 6 | 0 ± 0 | 0 ± 0 | 0 ± 0 | 2 ± 2 |
| TOTAL | 29470 ± 820 | 80170 ± 240 | 32800 ± 180 | 11852 ± 44 | 63010 ± 790 |

Table A2. MOR popping rock 2ΠD43 crush.

| crush step [no.] | $^{36}Ar\ 10^{-12}$ | $^{37}Ar\ 10^{-12}$ | $^{38}Ar\ 10^{-12}$ | $^{39}Ar\ 10^{-12}$ | $^{40}Ar\ 10^{-9}$ |
|---|---|---|---|---|---|
| 1 | 45 ± 3 | 0 ± 0 | 11 ± 2 | 4 ± 1 | 482 ± 13 |
| 2 | 19530 ± 510 | 0 ± 0 | 3781 ± 99 | 41 ± 8 | 33740 ± 880 |
| 3 | 12 ± 2 | 0 ± 0 | 5 ± 2 | 8 ± 2 | 170 ± 4 |
| 4 | 1532 ± 40 | 0 ± 0 | 302 ± 8 | 15 ± 3 | 7560 ± 200 |
| 5 | 39 ± 2 | 0 ± 0 | 9 ± 2 | 9 ± 2 | 1046 ± 13 |
| 6 | 54 ± 2 | 0 ± 0 | 10 ± 2 | 4 ± 2 | 1451 ± 18 |
| 7 | 24 ± 2 | 2 ± 2 | 6 ± 2 | 7 ± 2 | 626 ± 8 |
| 8 | 31 ± 2 | 0 ± 0 | 9 ± 2 | 9 ± 2 | 634 ± 8 |
| 9 | 5 ± 2 | 0 ± 0 | 3 ± 2 | 4 ± 2 | 172 ± 2 |
| 10 | 14 ± 2 | 0 ± 0 | 8 ± 2 | 6 ± 2 | 364 ± 4 |
| TOTAL | 21280 ± 510 | 2 ± 2 | 4144 ± 99 | 105 ± 10 | 46240 ± 900 |

Table A3. MORB glass 2ΠD40.

| Temp. [°C] | $^{36}Ar\ 10^{-13}$ | $^{37}Ar\ 10^{-12}$ | $^{38}Ar\ 10^{-13}$ | $^{39}Ar\ 10^{-14}$ | $^{40}Ar\ 10^{-10}$ |
|---|---|---|---|---|---|
| 320 | 4 ± 2 | 2 ± 1 | 0 ± 0 | 10 ± 10 | 1 ± 1 |
| 470 | 5 ± 2 | 3 ± 1 | 53 ± 15 | 1 ± 1 | 1 ± 1 |
| 620 | 2 ± 2 | 18 ± 4 | 182 ± 37 | 91 ± 46 | 2 ± 1 |
| 680 | 6 ± 3 | 27 ± 3 | 128 ± 11 | 85 ± 33 | 6 ± 1 |
| 740 | 3 ± 3 | 42 ± 2 | 119 ± 7 | 52 ± 32 | 11 ± 1 |
| 780 | 8 ± 3 | 71 ± 2 | 73 ± 2 | 164 ± 33 | 103 ± 1 |
| 820 | 6 ± 3 | 136 ± 2 | 81 ± 4 | 165 ± 24 | 127 ± 1 |
| 860 | 6 ± 3 | 179 ± 3 | 71 ± 4 | 160 ± 36 | 79 ± 1 |
| 900 | 2 ± 2 | 307 ± 7 | 69 ± 3 | 274 ± 41 | 39 ± 1 |
| 950 | 9 ± 3 | 576 ± 9 | 121 ± 4 | 550 ± 56 | 70 ± 1 |
| 1020 | 74 ± 4 | 851 ± 9 | 226 ± 4 | 726 ± 65 | 301 ± 3 |
| 1100 | 436 ± 40 | 44760 ± 390 | 5459 ± 55 | 36800 ± 2940 | 12120 ± 100 |
| 1180 | 41 ± 8 | 3068 ± 30 | 458 ± 7 | 2650 ± 210 | 501 ± 5 |
| 1260 | 232 ± 42 | 45330 ± 410 | 5710 ± 58 | 37530 ± 2980 | 5637 ± 49 |
| 1360 | 9 ± 9 | 791 ± 91 | 93 ± 14 | 680 ± 100 | 94 ± 11 |
| 1460 | 19 ± 19 | 55 ± 55 | 0 ± 0 | 55 ± 55 | 7 ± 7 |
| TOTAL | 861 ± 63 | 96220 ± 580 | 12842 ± 92 | 79990 ± 4190 | 19100 ± 120 |

Table A4. MORB glass CYP7806-11.

| Temp. [°C] | $^{36}$Ar $10^{-13}$ | $^{37}$Ar $10^{-12}$ | $^{38}$Ar $10^{-13}$ | $^{39}$Ar $10^{-13}$ | $^{40}$Ar $10^{-10}$ |
|---|---|---|---|---|---|
| 320 | 1 ± 1 | 0 ± 0 | 3 ± 3 | 1 ± 1 | 0 ± 0 |
| 420 | 3 ± 2 | 0 ± 0 | 5 ± 3 | 4 ± 3 | 1 ± 1 |
| 520 | 5 ± 2 | 1 ± 1 | 11 ± 2 | 10 ± 2 | 2 ± 1 |
| 600 | 1 ± 1 | 3 ± 1 | 6 ± 3 | 7 ± 3 | 1 ± 1 |
| 650 | 1 ± 1 | 3 ± 2 | 4 ± 3 | 5 ± 4 | 0 ± 0 |
| 700 | 2 ± 2 | 4 ± 4 | 3 ± 3 | 1 ± 1 | 0 ± 0 |
| 750 | 2 ± 2 | 10 ± 1 | 8 ± 1 | 6 ± 1 | 8 ± 1 |
| 800 | 70 ± 3 | 183 ± 1 | 144 ± 2 | 45 ± 2 | 1137 ± 1 |
| 850 | 324 ± 6 | 5995 ± 19 | 3668 ± 13 | 1020 ± 40 | 6723 ± 8 |
| 901 | 556 ± 18 | 18323 ± 57 | 12221 ± 41 | 3390 ± 120 | 4813 ± 5 |
| 950 | 306 ± 19 | 21443 ± 67 | 14292 ± 43 | 3990 ± 140 | 1811 ± 2 |
| 1000 | 117 ± 13 | 13765 ± 61 | 9129 ± 39 | 2529 ± 91 | 390 ± 1 |
| 1050 | 74 ± 9 | 8359 ± 72 | 5634 ± 49 | 1574 ± 56 | 172 ± 1 |
| 1100 | 22 ± 7 | 4830 ± 100 | 2968 ± 63 | 813 ± 36 | 86 ± 2 |
| 1160 | 63 ± 17 | 18360 ± 230 | 12180 ± 150 | 3370 ± 130 | 272 ± 3 |
| 1220 | 59 ± 13 | 4130 ± 230 | 2440 ± 130 | 678 ± 46 | 64 ± 4 |
| 1290 | 28 ± 28 | 74 ± 43 | 58 ± 34 | 57 ± 33 | 18 ± 10 |
| 1370 | 97 ± 97 | 19 ± 15 | 20 ± 20 | 9 ± 7 | 27 ± 20 |
| 1450 | 140 ± 140 | 1 ± 1 | 21 ± 21 | 2 ± 2 | 38 ± 27 |
| 1530 | 9 ± 9 | 1 ± 1 | 4 ± 4 | 5 ± 5 | 2 ± 2 |
| TOTAL | 1870 ± 170 | 95510 ± 370 | 62820 ± 230 | 17520 ± 260 | 15566 ± 37 |

Table A5. CYP7806-11 crush.

| crush step [no.] | $^{36}$Ar $10^{-13}$ | $^{37}$Ar $10^{-12}$ | $^{38}$Ar $10^{-13}$ | $^{39}$Ar $10^{-13}$ | $^{40}$Ar $10^{-10}$ |
|---|---|---|---|---|---|
| #1 1 | 135 ± 6 | 2 ± 1 | 32 ± 3 | 9 ± 4 | 118 ± 2 |
| 2 | 151 ± 7 | 0 ± 0 | 31 ± 3 | 15 ± 5 | 475 ± 6 |
| 3 | 226 ± 6 | 2 ± 1 | 48 ± 4 | 18 ± 5 | 517 ± 6 |
| 4 | 22 ± 7 | 2 ± 1 | 6 ± 6 | 21 ± 6 | 202 ± 3 |
| 5 | 39 ± 6 | 2 ± 1 | 30 ± 6 | 13 ± 4 | 632 ± 8 |
| 6 | 29 ± 6 | 3 ± 1 | 10 ± 10 | 8 ± 4 | 476 ± 6 |
| 7 | 32 ± 8 | 2 ± 1 | 16 ± 5 | 13 ± 6 | 428 ± 5 |
| 8 | 42 ± 5 | 3 ± 1 | 15 ± 5 | 7 ± 4 | 717 ± 16 |
| #2 1 | 76 ± 6 | 1 ± 1 | 28 ± 4 | 7 ± 4 | 1194 ± 27 |
| 2 | 60 ± 5 | 1 ± 1 | 19 ± 4 | 12 ± 4 | 1139 ± 26 |
| 3 | 88 ± 5 | 2 ± 1 | 21 ± 4 | 14 ± 4 | 985 ± 8 |
| 4 | 64 ± 8 | 8 ± 2 | 19 ± 4 | 11 ± 5 | 1273 ± 10 |
| TOTAL | 965 ± 22 | 28 ± 4 | 274 ± 18 | 149 ± 16 | 8156 ± 45 |

Table A6. MORB glass 2ПD44.

| Temp. [°C] | $^{36}$Ar $10^{-13}$ | $^{37}$Ar $10^{-12}$ | $^{38}$Ar $10^{-12}$ | $^{39}$Ar $10^{-12}$ | $^{40}$Ar $10^{-11}$ |
|---|---|---|---|---|---|
| 320 | 1 ± 1 | 0 ± 0 | 0 ± 0 | 1 ± 1 | 2 ± 2 |
| 390 | 4 ± 4 | 1 ± 1 | 0 ± 0 | 0 ± 0 | 9 ± 9 |
| 460 | 4 ± 4 | 1 ± 1 | 1 ± 1 | 0 ± 0 | 15 ± 11 |
| 530 | 5 ± 5 | 2 ± 2 | 3 ± 2 | 1 ± 1 | 13 ± 11 |
| 600 | 11 ± 6 | 6 ± 3 | 17 ± 8 | 1 ± 1 | 23 ± 11 |
| 690 | 85 ± 4 | 31 ± 1 | 47 ± 1 | 7 ± 1 | 5506 ± 55 |
| 730 | 25 ± 4 | 23 ± 1 | 26 ± 1 | 4 ± 1 | 1689 ± 89 |
| 770 | 36 ± 4 | 41 ± 2 | 40 ± 2 | 7 ± 1 | 4500 ± 230 |
| 810 | 194 ± 11 | 57 ± 3 | 39 ± 2 | 8 ± 1 | 1624 ± 85 |
| 850 | 35 ± 4 | 121 ± 6 | 68 ± 4 | 18 ± 1 | 1923 ± 100 |
| 890 | 39 ± 5 | 332 ± 17 | 165 ± 9 | 50 ± 3 | 3400 ± 180 |
| 930 | 22390 ± 1140 | 1759 ± 89 | 1132 ± 58 | 252 ± 13 | 67070 ± 3400 |
| 970 | 766 ± 41 | 8520 ± 440 | 3510 ± 180 | 1318 ± 68 | 5130 ± 260 |
| 1050 | 329 ± 23 | 13240 ± 790 | 5050 ± 300 | 2010 ± 120 | 3000 ± 170 |
| 1090 | 80 ± 10 | 5790 ± 510 | 1940 ± 170 | 780 ± 69 | 717 ± 57 |
| 1140 | 53 ± 22 | 22210 ± 3050 | 8100 ± 1110 | 3270 ± 450 | 1010 ± 140 |
| 1190 | 80 ± 20 | 18480 ± 2550 | 5800 ± 800 | 2520 ± 350 | 840 ± 120 |
| 1250 | 46 ± 12 | 4970 ± 940 | 1190 ± 230 | 550 ± 110 | 280 ± 53 |
| 1310 | 150 ± 31 | 416 ± 79 | 57 ± 11 | 28 ± 5 | 439 ± 84 |
| 1380 | 190 ± 100 | 145 ± 54 | 5 ± 3 | 0 ± 0 | 570 ± 210 |
| TOTAL | 24530 ± 1150 | 76140 ± 4220 | 27190 ± 1440 | 10840 ± 600 | 97750 ± 3440 |

Table A7. 2ПD44 crush.

| crush step [no.] | $^{36}$Ar $10^{-13}$ | $^{37}$Ar $10^{-13}$ | $^{38}$Ar $10^{-13}$ | $^{39}$Ar $10^{-13}$ | $^{40}$Ar $10^{-11}$ |
|---|---|---|---|---|---|
| 1 | 7 ± 3 | 15 ± 9 | 6 ± 3 | 5 ± 3 | 288 ± 6 |
| 2 | 1119 ± 18 | 110 ± 13 | 267 ± 7 | 64 ± 6 | 7930 ± 120 |
| 3 | 7 ± 3 | 19 ± 9 | 8 ± 3 | 7 ± 3 | 237 ± 6 |
| 4 | 26 ± 3 | 3 ± 3 | 16 ± 4 | 18 ± 6 | 2291 ± 36 |
| 5 | 20 ± 3 | 99 ± 10 | 57 ± 3 | 25 ± 4 | 1304 ± 21 |
| TOTAL | 1179 ± 19 | 246 ± 21 | 354 ± 10 | 119 ± 10 | 12050 ± 130 |

Table A8. Loihi S2335-6 glass.

| Temp. [°C] | $^{36}$Ar $10^{-13}$ | $^{37}$Ar $10^{-12}$ | $^{38}$Ar $10^{-12}$ | $^{39}$Ar $10^{-13}$ | $^{40}$Ar $10^{-11}$ |
|---|---|---|---|---|---|
| 320 | 0 ± 0 | 0 ± 0 | 0 ± 0 | 0 ± 0 | 0 ± 0 |
| 470 | 148 ± 3 | 3 ± 1 | 10 ± 1 | 6 ± 2 | 411 ± 4 |
| 620 | 22 ± 3 | 12 ± 1 | 29 ± 2 | 17 ± 3 | 61 ± 3 |
| 690 | 17 ± 2 | 31 ± 1 | 46 ± 1 | 57 ± 4 | 1137 ± 4 |
| 760 | 6 ± 2 | 479 ± 5 | 542 ± 6 | 838 ± 11 | 320 ± 4 |
| 820 | 14 ± 3 | 3176 ± 27 | 3024 ± 25 | 4749 ± 45 | 433 ± 4 |
| 880 | 43 ± 5 | 10115 ± 30 | 9632 ± 28 | 15418 ± 81 | 1740 ± 5 |
| 940 | 42 ± 5 | 6799 ± 54 | 6456 ± 52 | 10356 ± 96 | 1457 ± 11 |
| 1000 | 28 ± 5 | 7170 ± 80 | 6801 ± 76 | 10990 ± 130 | 1006 ± 11 |
| 1080 | 79 ± 9 | 19450 ± 140 | 20250 ± 140 | 32710 ± 260 | 3014 ± 20 |
| 1160 | 42 ± 7 | 1306 ± 74 | 684 ± 39 | 1172 ± 67 | 308 ± 17 |
| 1240 | 56 ± 18 | 5330 ± 820 | 42 ± 6 | 56 ± 36 | 282 ± 43 |
| 1340 | 0 ± 0 | 4830 ± 1840 | 16 ± 6 | 20 ± 20 | 450 ± 170 |
| 1440 | 0 ± 0 | 280 ± 280 | 6 ± 6 | 1 ± 1 | 250 ± 250 |
| 1530 | 0 ± 0 | 0 ± 0 | 0 ± 0 | 0 ± 0 | 0 ± 0 |
| TOTAL | 497 ± 31 | 58990 ± 2040 | 47540 ± 170 | 76380 ± 330 | 10880 ± 310 |

Table A9. Loihi S2335-6 glass crush.

| crush step [no.] | $^{36}$Ar $10^{-14}$ | $^{37}$Ar $10^{-12}$ | $^{38}$Ar $10^{-13}$ | $^{39}$Ar $10^{-13}$ | $^{40}$Ar $10^{-11}$ |
|---|---|---|---|---|---|
| 1 | 119 ± 89 | 0 ± 0 | 5 ± 5 | 11 ± 9 | 38 ± 12 |
| 2 | 0 ± 0 | 1 ± 1 | 0 ± 0 | 0 ± 0 | 38 ± 7 |
| 3 | 240 ± 65 | 2 ± 2 | 26 ± 6 | 16 ± 6 | 315 ± 12 |
| 4 | 197 ± 83 | 8 ± 2 | 52 ± 7 | 25 ± 7 | 1466 ± 17 |
| 5 | 2 ± 2 | 2 ± 2 | 25 ± 10 | 8 ± 7 | 42 ± 12 |
| TOTAL | 560 ± 140 | 14 ± 3 | 108 ± 15 | 60 ± 14 | 1899 ± 28 |

Table A10. Loihi S2335-10 glass.

| Temp. [°C] | $^{36}$Ar $10^{-13}$ | $^{37}$Ar $10^{-12}$ | $^{38}$Ar $10^{-12}$ | $^{39}$Ar $10^{-13}$ | $^{40}$Ar $10^{-11}$ |
|---|---|---|---|---|---|
| 320 | 9 ± 2 | 1 ± 1 | 1 ± 1 | 0 ± 0 | 29 ± 2 |
| 470 | 9 ± 2 | 3 ± 1 | 4 ± 1 | 7 ± 2 | 37 ± 2 |
| 620 | 10 ± 2 | 10 ± 1 | 13 ± 1 | 21 ± 2 | 34 ± 2 |
| 690 | 8 ± 2 | 20 ± 2 | 21 ± 2 | 39 ± 4 | 30 ± 2 |
| 760 | 2 ± 2 | 124 ± 7 | 118 ± 6 | 193 ± 11 | 38 ± 2 |
| 820 | 22 ± 3 | 2655 ± 38 | 2140 ± 31 | 3836 ± 57 | 508 ± 7 |
| 880 | 39 ± 7 | 6830 ± 96 | 5476 ± 77 | 10070 ± 150 | 984 ± 14 |
| 940 | 94 ± 13 | 13670 ± 220 | 10990 ± 180 | 20300 ± 340 | 2038 ± 30 |
| 1000 | 45 ± 7 | 5340 ± 110 | 4281 ± 86 | 7860 ± 160 | 821 ± 17 |
| 1060 | 71 ± 17 | 18320 ± 280 | 14680 ± 220 | 27190 ± 430 | 2467 ± 37 |
| 1140 | 78 ± 8 | 5550 ± 120 | 4470 ± 97 | 8310 ± 190 | 988 ± 21 |
| 1220 | 87 ± 14 | 2950 ± 280 | 103 ± 10 | 199 ± 27 | 342 ± 32 |
| 1300 | 109 ± 33 | 7510 ± 1270 | 42 ± 7 | 17 ± 17 | 466 ± 79 |
| 1400 | 0 ± 0 | 3810 ± 3810 | 42 ± 42 | 10 ± 10 | 180 ± 180 |
| TOTAL | 581 ± 44 | 66800 ± 4040 | 42380 ± 330 | 78040 ± 620 | 8960 ± 210 |

Table A11. Loihi S2335-10 glass crush.

| crush step [no.] | $^{36}$Ar $10^{-13}$ | $^{37}$Ar $10^{-12}$ | $^{38}$Ar $10^{-13}$ | $^{39}$Ar $10^{-13}$ | $^{40}$Ar $10^{-11}$ |
|---|---|---|---|---|---|
| 1 | 4 ± 3 | 1 ± 1 | 9 ± 4 | 12 ± 4 | 17 ± 4 |
| 2 | 11 ± 4 | 3 ± 1 | 6 ± 3 | 21 ± 5 | 23 ± 5 |
| 3 | 6 ± 3 | 0 ± 0 | 9 ± 5 | 21 ± 3 | 86 ± 4 |
| 4 | 35 ± 3 | 8 ± 1 | 54 ± 4 | 8 ± 3 | 149 ± 4 |
| TOTAL | 56 ± 6 | 11 ± 2 | 77 ± 8 | 63 ± 7 | 276 ± 8 |

Table A12. Loihi S2341-2 glass.

| Temp. [°C] | $^{36}$Ar $10^{-13}$ | $^{37}$Ar $10^{-12}$ | $^{38}$Ar $10^{-12}$ | $^{39}$Ar $10^{-12}$ | $^{40}$Ar $10^{-10}$ |
|---|---|---|---|---|---|
| 320 | 0 ± 0 | 0 ± 0 | 0 ± 0 | 0 ± 0 | 0 ± 0 |
| 470 | 3952 ± 24 | 9 ± 2 | 155 ± 1 | 4 ± 1 | 1150 ± 5 |
| 620 | 33960 ± 190 | 53 ± 2 | 954 ± 5 | 14 ± 1 | 10164 ± 42 |
| 660 | 3010 ± 19 | 44 ± 2 | 241 ± 2 | 12 ± 1 | 918 ± 4 |
| 700 | 825 ± 9 | 1384 ± 10 | 1890 ± 11 | 327 ± 2 | 495 ± 2 |
| 750 | 34 ± 5 | 2435 ± 34 | 2409 ± 33 | 557 ± 8 | 78 ± 1 |
| 800 | 335 ± 7 | 4273 ± 34 | 4289 ± 33 | 983 ± 8 | 168 ± 1 |
| 850 | 49 ± 11 | 11050 ± 160 | 10790 ± 160 | 2542 ± 38 | 73 ± 1 |
| 910 | 67 ± 7 | 5570 ± 160 | 5330 ± 160 | 1282 ± 39 | 37 ± 1 |
| 970 | 12 ± 7 | 3650 ± 460 | 3510 ± 450 | 820 ± 110 | 13 ± 2 |
| 1040 | 46 ± 19 | 16940 ± 970 | 16480 ± 950 | 3910 ± 230 | 51 ± 3 |
| 1130 | 54 ± 32 | 21020 ± 2470 | 20030 ± 2360 | 4780 ± 560 | 61 ± 7 |
| 1220 | 71 ± 47 | 11750 ± 5150 | 560 ± 250 | 148 ± 66 | 22 ± 10 |
| 1370 | 3 ± 3 | 3700 ± 3700 | 24 ± 24 | 6 ± 6 | 0 ± 0 |
| TOTAL | 42420 ± 200 | 81860 ± 6900 | 66670 ± 2600 | 15390 ± 620 | 13230 ± 44 |

Table A13. Loihi S2341-2 glass crush.

| crush step [no.] | $^{36}$Ar $10^{-13}$ | $^{37}$Ar $10^{-12}$ | $^{38}$Ar $10^{-13}$ | $^{39}$Ar $10^{-13}$ | $^{40}$Ar $10^{-10}$ |
|---|---|---|---|---|---|
| 1 | 5696 ± 17 | 0 ± 0 | 1069 ± 11 | 20 ± 8 | 1687 ± 2 |
| 2 | 1287 ± 9 | 3 ± 1 | 514 ± 8 | 3 ± 3 | 424 ± 1 |
| 3 | 22087 ± 58 | 2 ± 1 | 5109 ± 17 | 27 ± 8 | 6568 ± 7 |
| 4 | 818 ± 6 | 5 ± 2 | 175 ± 6 | 40 ± 9 | 295 ± 1 |
| 5 | 16 ± 5 | 4 ± 1 | 15 ± 6 | 0 ± 0 | 95 ± 2 |
| 6 | 0 ± 0 | 1 ± 1 | 13 ± 6 | 2 ± 2 | 8 ± 1 |
| 7 | 6563 ± 91 | 10 ± 2 | 1353 ± 21 | 26 ± 7 | 2136 ± 29 |
| TOTAL | 36470 ± 110 | 26 ± 4 | 8248 ± 32 | 118 ± 16 | 11212 ± 30 |